

1

2 Foreland magmatism during the Arabia – Eurasia collision:
3 Pliocene-Quaternary activity of the Karacadağ Volcanic
4 Complex, SW Turkey

5

6 Taner Ekici^{1*}, Colin G. Macpherson², Nazmi Otlu¹, Denis Fontignie³

7

8 ¹ Department of Geological Engineering, University of Cumhuriyet, 58140, Sivas,
9 Turkey

10 ² Department of Earth Sciences, University of Durham, Durham, DH1 3LE, UK.

11 ³ Department of Mineralogy, University of Geneva, CH-1205 Geneva, Switzerland.

12

13 * Corresponding author:
14 tanere7@gmail.com
15 Tel: +903462191010/1928
16 Fax: +902191171

17

18

19

20

Running Title: Quaternary Petrogenesis of Mt. Karacadağ

21

22

23

24

25

Submitted draft for *Journal of Petrology*

26

13 May 2014

27

28

29

30

ABSTRACT

31 Pliocene to Quaternary magmatism in the Karacadağ Volcanic Complex in southeast
32 Turkey occurred in the foreland region of the Arabia - Eurasia collision and can be
33 divided into two phases. The earlier Karacadağ phase formed a north-south trending
34 volcanic ridge that erupted three groups of lavas. The same range of mantle sources
35 contributed to the younger Ovabağ phase lavas which were erupted from
36 monogenetic cones to the east of the Karacadağ fissure. Like several other intraplate
37 localities across the northern Arabian Plate this magmatism represents mixtures of
38 melt from shallow, isotopically enriched mantle and from deeper, more depleted
39 mantle. The deep source is similar to the depleted mantle invoked for other northern
40 Arabian intraplate volcanic fields but at Karacadağ this source contained phlogopite.
41 This source could be located in the shallow convecting mantle or may represent a
42 metasomatic layer in the base of the lithosphere. There is no evidence for a
43 contribution from the Afar mantle plume, as has been proposed elsewhere in
44 northern Arabia. Melting during the Karacadağ and Ovabağ phases could have
45 resulted from a combination of upwelling beneath weak or thinned lithosphere and
46 restricted local extension of that weakened lithosphere as it collided with Eurasia.
47 Tension associated with the collision focussed magma of the Karacadağ phase into
48 the elongate shield volcano of Mt. Karacadağ. The northern end of the fissure
49 accommodated more extensive differentiation of magma, with isolated cases of
50 crustal contamination, consistent with greater stress in the lithosphere closest to the
51 collision. Most magma batches of the Karacadağ and Ovabağ phases differentiated
52 by fractional crystallisation at ~ 5 MPa, near the boundary between the upper and
53 lower crust. Magma batches dominated by melt from garnet lherzolite show evidence
54 for restricted amounts of differentiation at ~ 22.5 MPa, which is close to the base of
55 the lithospheric mantle.

56 Keywords: Arabia; fissure volcano; intraplate; Karacadağ; Turkey.

57

58

INTRODUCTION

59 The Arabian Plate hosts several basaltic volcanic fields and so provides a valuable
60 natural laboratory to explore intraplate magmatism (Camp and Roobol 1992; Ilani et
61 al., 2001; Shaw et al., 2003; Krienitz et al., 2006, 2007 and 2009; Ma et al., 2011).
62 Intraplate magmatism occurred in clusters from 30 to 16 Ma and/or from 13 to 8 Ma
63 in southern Turkey (e.g. Gaziantep, Kilis, Karacadağ; Gürsoy et al., 2009; Lustrino et
64 al., 2010 and 2012; Ekici et al., 2012), in northern Syria (Krienitz et al., 2006), in the
65 Syrian Dead Sea Fault (Ma et al., 2011) and in the Harrat Ash Shaam (Shaw et al.,
66 2003; Krienitz et al., 2007), with a significant increase in activity since the Pliocene
67 (Ilani et al., 2001). Most of this activity occurred close to and parallel to, although not
68 always within, tectonic structures such as the Dead Sea Fault Zone, Euphrates
69 Graben, Sirhan Graben, Karak Graben and Esdraelon Valley (Fig. 1a). Some of
70 these structures, for example the Euphrates Graben, experienced no tectonic activity
71 during magmatism.

72 The Karacadağ Volcanic Complex in southeast Turkey (Fig. 1), sometimes referred
73 to as Karacalıdağ, is one of a number of such fields distributed along the northern
74 edge of the Arabian Plate, where it has collided with Anatolia (Allen et al., 2004).
75 Until recently, magmatism from this complex was reported to be very young (Pearce
76 et al., 1990; Şen et al., 2004). New geochronological data for the Siverek plateau
77 lavas, which constitute the earliest activity of the complex, indicate that activity
78 began no later than the Middle Miocene (Lustrino et al., 2010 and 2012; Ekici et al.,
79 2012). Petrogenetic models for the Karacadağ Volcanic Complex, and for other
80 intraplate fields in northernmost Arabia, have tended to concentrate on the proximity
81 of the Arabian – Anatolian collision in seeking a geodynamic context for magmatism
82 (e.g. Keskin, 2003; Krientiz et al., 2006). The recognition of multiple phases of
83 magmatism demonstrates that the Karacadağ Volcanic Complex is not the result of a
84 single event or process. In a previous publication we discussed the petrogenesis of

85 the Miocene Siverek plateau lavas (Ekici et al., 2012). In this contribution we turn our
86 attention to the younger magmatism. Lustrino et al. (2012) have shown this is
87 geochemically distinct from the earlier Siverek phase. Our analysis reveals further
88 levels of distinction within each of the two young phases of activity at the complex.
89 We explore the genesis and differentiation of this magmatism in the context of
90 tectonic activity associated with the developing collision and the structure of the
91 Arabian Plate.

92

GEOLOGICAL SETTING

93 The Karacadağ Volcanic Complex, in southeast Turkey, lies immediately south of the
94 Arabian – Anatolian Collision Zone (Fig. 1). The collision is the result of northward
95 motion of the Arabian Plate, with respect to Eurasia and the Anatolian Plate (Allen et
96 al., 2004). During the Paleocene this caused Neo-Tethyan oceanic lithosphere to be
97 subducted beneath Anatolia. Subduction continued until formation of the Bitlis Suture
98 between Arabia and Anatolia (Fig. 1a). Continued convergence between Arabia and
99 Eurasia led to westward extrusion of Anatolia along the Northern- and Eastern
100 Anatolian faults during the Late Miocene (Robertson, 2000; Şengör et al., 2008).

101 The structure of the northernmost Arabian Plate is relatively poorly known, with most
102 constraints coming from studies in Saudi Arabia, Jordan and Syria. Heat flow
103 measurements and xenolith petrology have been used to estimate that the
104 lithosphere – asthenosphere transition occurs at approximately 80 km depth
105 (McGuire and Bohannon, 1989; Nasir and Safarjalani, 2000; Shaw et al., 2007).
106 Seismic data suggest that beneath 35 km depth a mafic, lower crust is succeeded by
107 a 5 to 8 km-thick mantle transition zone (El-Isa et al., 1987a, b). Both petrologic and
108 seismic evidence indicate that a boundary between upper and lower crust lies close
109 to 19 km beneath the surface (El-Isa et al., 1987b; Nasir, 1992).

110 The Karacadağ Volcanic Complex has been active since the Middle Miocene when
111 the Siverek phase plateau basalts were produced (Ercan et al., 1990; Lustrino et al.,

112 2010; Ekici et al., 2012) but is particularly well known for its Late Miocene to
113 Quaternary products (Pearce et al., 1990; Ercan et al., 1990; Adiyaman and
114 Chorowicz, 2002; Keskin, 2003; Şen et al., 2004; Brigland et al., 2007; Demir et al.,
115 2007; Lustrino et al., 2010). This younger activity can be grouped into two further
116 phases, termed Karacadağ and Ovabağ.

117 During the Late Miocene to Quaternary alkali basaltic and basanitic lavas were
118 erupted from Mt. Karacadağ, a north-south fissure volcano approximately 25 km in
119 length. We refer to three summits on the volcanic axis as the northern, central and
120 southern summits (Fig. 1b). Individual lavas from Mt Karacadağ initially flowed east
121 or west, extending up to 15 km to either side of the volcanic ridge. The lava fields
122 also extend up to 25 km north and south of the fissure. Nine Ar-Ar measurements
123 yield ages ranging from 4.50 to 0.91 Ma (Ekici et al., submitted), which agree with
124 prior radiometric measurements for Mt. Karacadağ (Pearce et al., 1990; Lustrino et
125 al., 2010). Adiyaman and Chorowicz (2002) have suggested that the northern end of
126 Mt. Karacadağ lies at the southern end of a WNW-ESE fault extending from the East
127 Anatolian Fault. The Karacadağ fissure indicates that the lithosphere was under
128 tensional stress during this stage of the collision, although there is little evidence that
129 this part of the northern margin of the Arabian Plate experienced significant east-
130 west extension.

131 Products of the youngest phase of activity in the complex lie approximately 15 km to
132 the east of Mt. Karacadağ, around the village of Ovabağ (Fig. 1b). These are
133 predominantly alkali basalt flows erupted from monogenetic cones and cover
134 approximately 150 km². The youngest of these flows, erupted from the 100m high
135 Baruttepe cone, is exceptionally fresh although there is little evidence of alteration of
136 any of the Ovabağ flows. Most of these were erupted from cones, similar to
137 Baruttepe, and flowed east up to 20 km from the eastern flank of Mt. Karacadağ
138 before being channelled into river valleys and flowing up to a further 5 km east or
139 southeast. The flows are vesicular and often retain flow structures such as pahoehoe

140 surfaces and surface break-out structures. Vesicles are generally empty and only
141 rarely contain secondary calcite. Similar monogenetic cones occur further to the east
142 and south of the Karacadağ Volcanic Complex, towards the border with Syria. Ekici
143 et al. (submitted) obtained an Ar-Ar ages of $0.29\text{Ma} \pm 0.13$ and $0.53\text{Ma} (\pm 1.14)$ for
144 an Ovabağ lava, which is consistent with the geomorphological evidence of very
145 recent activity.

146 ANALYTICAL METHODS

147 Seventy-six fresh samples, forty-eight from Mt. Karacadağ and twenty-eight from
148 Ovabağ, were analysed for major and trace element concentrations at ACME
149 laboratories (Canada; Table 1). Any calcite-bearing vesicles were avoided when
150 preparing material for analysis. Major element analyses were conducted by X-ray
151 fluorescence upon fused discs prepared by using six parts of lithium tetraborate and
152 one part of rock powder. The mixture was fused in crucibles of 95% Pt and 5% Au at
153 1050°C for 60 minutes to form a homogeneous melt that was cast into a thick glass
154 disc. Trace element concentrations were analysed by ICP-MS using a fusion
155 method. Precision was monitored using an internal standard (SO-18) while accuracy
156 was calibrated using standards W-2, GSP-2, BCR-2, SY4 and SY-3 (Supplementary
157 Tables 1 & 2). Uncertainty on these measurements is better than $\pm 3\%$ for major
158 element oxides and $\pm 10\%$ for trace elements.

159 Isotope ratios of Pb, Sr, and Nd were measured on splits separated from the same
160 0.2 g aliquots at the University of Geneva using a 7-collector Finnigan MAT 262
161 thermal ionisation mass spectrometer during December 2008. Samples were
162 processed using procedures described in Chiaradia et al. (2011). The 90° magnetic
163 sector mass analyser has an extended geometry with stigmatic focusing. $^{87}\text{Sr}/^{86}\text{Sr}$
164 and $^{143}\text{Nd}/^{144}\text{Nd}$ ratios were measured in semi-dynamic mode, using double Re
165 filaments. Conventional Pb isotope ratio measurements were obtained in dynamic
166 mode with a single Re filament. $^{88}\text{Sr}/^{86}\text{Sr} = 8.375209$ was used to correct the mass

167 fractionation of $^{87}\text{Sr}/^{86}\text{Sr}$, which was compared to the NIST-SRM987 $^{87}\text{Sr}/^{86}\text{Sr}$ value
168 of 0.710240 ($^{87}\text{Sr}/^{86}\text{Sr}_{\text{measured}} = 0.710240 \pm 0.000012$ (2σ), $n = 31$). $^{143}\text{Nd}/^{144}\text{Nd}$ was
169 mass fractionation corrected relative to a $^{146}\text{Nd}/^{144}\text{Nd}$ value of 0.721903 and
170 normalized to the Nd La Jolla standard value of 0.511835 ($^{143}\text{Nd}/^{144}\text{Nd}_{\text{measured}} =$
171 0.511845 ± 0.000004 (2σ), $n = 26$). Lead isotope data were corrected for
172 instrumental mass fractionation and machine bias by applying a discrimination factor
173 determined by multiple analyses of NBS SRM981, using the reference value of Todt
174 et al. (1984). The discrimination factor averaged 0.00082 ± 0.00005 (2 SE , $n = 132$)
175 per mass unit. External reproducibility (2σ) of the standard ratios are 0.05% for
176 $^{206}\text{Pb}/^{204}\text{Pb}$, 0.08% for $^{207}\text{Pb}/^{204}\text{Pb}$ and 0.10% for $^{208}\text{Pb}/^{204}\text{Pb}$. These standard
177 analyses were performed during a 6-month period in which the Karacadağ lavas
178 were analysed. Pb, Sr and Nd blanks were all below their respective detection limits.

179 RESULTS

180 Petrography

181 All lavas from Mt. Karacadağ itself are alkaline, being alkali basalts, trachybasalts,
182 basanites and tephrites, with rare phonotephrite. Most lavas are very fresh, the vast
183 majority having low Loss on Ignition (LOI) values of less than 1 % (Table 1). The
184 lavas are fine grained and porphyritic, containing olivine and plagioclase
185 phenocrysts, up to 25 modal %, set in a matrix of the same minerals, plus
186 clinopyroxene, which is occasionally titanium-rich and oxides. Phenocrysts are
187 generally 0.2 – 1 mm in size with groundmass crystals less than 0.1 mm. Plagioclase
188 phenocrysts show some signs of disequilibrium with sieve textures observed in a
189 number of samples. Such disequilibrium might arise from magma-mixing or
190 contamination (Dungan and Rhodes, 1978) but could also result from decompression
191 or heating (Nelson and Montana 1992; Thy et al., 2013). Therefore, the sieve
192 textures, in themselves, do not provide evidence for open system behaviour.

193 Lavas from Ovabağ are exceptionally fresh as shown by their very low, and
194 frequently positive, LOI, which is due to iron oxidation during ignition. These lavas
195 include basalts, alkali basalts, trachybasalts and rare tephrites. Like Karacadağ
196 phase lavas these are fine-grained flows but differ in the predominance of olivine
197 phenocrysts. Again, there is a range of phenocryst contents, up to 25 modal %.
198 Titanite is more common than at Karacadağ, sometimes as micro-phenocrysts,
199 but usually as part of the groundmass.

200 **Results**

201 Lavas from both phases can be split into three groups based on geochemistry. In the
202 discussion below these are referred to as groups K1, K2 and K3 for the Karacadağ
203 Phase and O1, O2 and O3 for the Ovabağ phase. Similarities between Karacadağ
204 groups and Ovabağ groups will be mentioned where appropriate.

205 *Karacadağ Phase*

206 Lavas from both the Karacadağ and Ovabağ phases show similar ranges of major
207 and trace element compositions to those observed by prior studies (Fig. 2 and 3).
208 Karacadağ phase lavas display a much wider range in compositions than those from
209 Ovabağ. Group K1 lavas have lower MgO (2.2 – 6.7 wt. %) and higher Al₂O₃ (> 15
210 wt. %) than the remaining two Karacadağ groups (Fig. 2). In groups K2 and K3 MgO
211 is generally greater than 8 wt. % but K3 is offset to lower SiO₂ and Al₂O₃ and to
212 higher TiO₂, Fe₂O₃, Na₂O, K₂O and P₂O₅ for any particular MgO content. Most major
213 element oxides correlate well with MgO, particularly in group K1, although Fe₂O₃ and
214 TiO₂ display more scatter than others due to an inflection at around 5 wt. % MgO.
215 The major element groupings of the Karacadağ phase are also readily apparent in
216 trace element concentrations. Nickel contents of K2 and K3 lavas are similar to one
217 another and significantly greater than those of K1 (Table 1). Within each group of the
218 Karacadağ phase concentrations of incompatible elements increase with decreasing
219 MgO (Fig. 3).

220 In mantle normalised plots all Karacadağ phase lavas show patterns that are
221 enriched in the most incompatible elements, peaking at Nb, and depleted in the
222 heavy rare earth elements and Y (Fig. 4). A striking negative Pb anomaly is apparent
223 in the patterns of all groups. Patterns for K1 and K2 lavas are very similar but with
224 greater concentrations in the former, consistent with their lower MgO contents.
225 Group K3 lavas have more elevated concentrations of incompatible elements than
226 those from group K2 (Fig. 2) but with similar shaped patterns (Fig. 4b and c), except
227 for the presence of negative K anomalies in most K3 samples. The magnitude of this
228 anomaly is not linked to MgO content but it is more pronounced in silica-poor rocks
229 (Fig. 5a and b).

230 Group K3 lavas display the lowest values of $^{87}\text{Sr}/^{86}\text{Sr}$ and $\Delta 7/4$ and $\Delta 8/4$, and the
231 highest values of $^{143}\text{Nd}/^{144}\text{Nd}$ (Table 2 and Fig. 6) of any lava from the Karacadağ
232 Volcanic Complex. Ratios for the other two Karacadağ groups largely overlap one
233 another but a K1 sample (DK-58) displays the most radiogenic Sr and least
234 radiogenic Nd isotopic ratios in this study. However, these values are not as extreme
235 as noted for the Miocene Siverek plateau lavas (Fig. 6). With the exception of DK-58,
236 the ranges of isotopic ratios are similar to those previously observed for intra-plate
237 magmatism elsewhere in the northern Arabian Plate (Shaw et al., 2003; Krienitz et
238 al., 2009; Ma et al., 2011).

239 *Ovabağ Phase*

240 All Ovabağ lavas contain more than 8 wt. % MgO. Group O1 lavas have higher SiO_2
241 and Al_2O_3 , and lower CaO, Fe_2O_3 , TiO_2 , K_2O and Na_2O than O3 lavas at similar
242 MgO. The restricted ranges in composition make it difficult to resolve systematic
243 variations of other major elements with MgO within each group. Group O2 lavas are
244 relatively scarce in our dataset and have the highest SiO_2 and lowest K_2O , TiO_2 ,
245 Na_2O for any MgO content in the Ovabağ phase (Fig. 2). Groups O1 and O3 display
246 parallel, negative correlations between MgO and Ni (not shown), while O3 lavas are

247 consistently enriched in incompatible elements compared to O1 at a particular MgO
248 content (Fig. 3). Group O2 lavas have the lowest incompatible element contents of
249 the Ovabağ groups.

250 Comparing the Ovabağ and Karacadağ phases with one another, concentrations of
251 major and incompatible trace elements in Group O1 lavas most closely resemble
252 Group K2 but possess slightly higher SiO₂ and K₂O (and most incompatible trace
253 elements), and lower Fe₂O₃ and TiO₂ (Fig. 2 and 3). Several O1 lavas also show
254 minor, positive K anomalies (Fig. 5b). The shapes of O2 lavas in the multi-element
255 plot are similar to O1 but, as noted above, have lower concentrations of all
256 incompatible elements (Fig. 4). The greatest distinction of group O3 from other
257 Ovabağ lavas is their negative K anomalies, which are not as pronounced as seen in
258 group K3 but are, again, associated with lower silica contents (Fig. 5b). Lavas from
259 groups K3 and O3 are very similar with respect to many major and trace elements
260 (Fig. 2 and 3) and trace element ratios (Fig. 4 and 5).

261 Lavas from the Ovabağ Phase of magmatism display more restricted ranges of
262 radiogenic isotope ratios than the Karacadağ Phase (Table 2). The lowest ⁸⁷Sr/⁸⁶Sr
263 and highest ¹⁴³Nd/¹⁴⁴Nd ratios occur in group O3, with values approaching those of
264 group K3 (Fig. 6). A lava from group O1 (DO-68) possesses Sr, Nd and Pb isotopic
265 ratios that lie within the range of the K1 and K2 lavas. The remaining Ovabağ lavas
266 have isotopic ratios that lie within the range previously observed for other northern
267 Arabian intraplate volcanic fields (Fig. 6).

268

DISCUSSION

269 The existence of multiple magmatic phases within the Karacadağ Volcanic Complex
270 has only been reported recently (Lustrino et al., 2010; Ekici et al., 2012). Previously,
271 the complex, along with its sources and causative mechanisms, was regarded as
272 having a short magmatic history (e.g. Pearce et al. 1990; Keskin, 2003). Lustrino et
273 al. (2012) recognised differences between the major and trace element geochemistry

274 of Karacadağ and Ovabağ phase lavas and attributed this to a long term secular
275 change in source compositions that included the preceding Siverek plateau lavas.
276 The range in $^{87}\text{Sr}/^{86}\text{Sr}$ that we have recognised is similar to that documented by
277 Lustrino et al. (2012) but offset to slightly lower values. Our new data reveal a
278 significantly larger range in $^{143}\text{Nd}/^{144}\text{Nd}$, largely due to the small number of samples
279 for which Lustrino et al. (2012) determined Nd isotopic ratios.

280 We have previously documented that much of the isotopic variation of the Siverek
281 lavas can be attributed to crustal contamination (Ekici et al., 2012). Our new data
282 reveal that there are significant variations in major and trace element chemistry
283 within both the Karacadağ and Ovabağ phases. For Mt. Karacadağ this variation
284 also involves a spatial aspect, with K1 lavas being clustered close to the northern
285 summit and K3 close to the central summit (Fig. 1b). Thus, before evaluating
286 changes in the mantle sources we must determine the role of differentiation,
287 including crustal contamination, in generating the chemical diversity of the
288 Karacadağ and Ovabağ lavas.

289 **Fractional Crystallisation**

290 Most lavas in this study possess relatively high MgO contents. The main exception to
291 this is group K1 in which MgO varies between 2.3 and 6.7 wt. %, suggesting
292 moderate to extensive differentiation of primary magma. Some K3 lavas also show
293 slightly more evolved compositions with MgO contents of c. 6 wt. %. To examine
294 whether fractional crystallisation could generate the variations within these groups
295 we undertook modelling using alphaMELTS software (Smith and Asimow, 2005).

296 The low MgO contents of K1 lavas suggest that none of these represent a parental
297 magma but most ratios of incompatible trace element in K1 lavas are very similar to
298 those of group K2 (Figs. 4 and 5). Therefore, we selected a primitive group K2 lava,
299 KD-102, as the starting composition with which to attempt to replicate variations
300 within group K1. For K3 lavas, which cannot be produced from a K2 parent, we

301 chose KD-26, the member of this group with the most elevated MgO. Relatively low
302 water contents (0.35 wt. %) were required for both parent compositions and the
303 oxygen fugacity was set at the QFM buffer. More extreme values for either of these
304 parameters failed to generate suitable models. Specifically, elevated fO_2 resulted in
305 early oxide saturation while more elevated H_2O suppressed plagioclase crystallisation
306 in lower pressure models. An iterative approach revealed that only a narrow range of
307 differentiation conditions replicated the compositional variation of each group.

308 Major element variations of group K1 can be replicated through fractional
309 crystallisation of KD-102 at 5 MPa. In this model the initial stages of crystallisation,
310 which account for removal of less than 10 % of the original mass of melt, are
311 dominated by olivine with minor spinel. This stage is able to generate much of the
312 major element variation observed in the K2 group, although there is some scatter of
313 the alkali and alkaline earth metals (see below). Group K1 closely resemble melts
314 generated after olivine is replaced on the liquidus by clinopyroxene at c. 7 wt. %
315 MgO (Fig. 7). The proportion of spinel crystallising in the 5 MPa model increases
316 significantly at 5 wt. % MgO, which corresponds to a significant inflection in TiO_2 ,
317 Fe_2O_3 and V in the K1 array (Fig. 3 and 7) although some groundmass
318 clinopyroxene in K1 lavas is titanite, which could also contribute to depletion of
319 these elements. At around 4 wt. % MgO the model precipitated plagioclase. This is
320 consistent with the very minor inflections for Al_2O_3 (Fig. 2 and 7) at which point
321 slightly less than 40% of the original melt had crystallised. The models are also
322 consistent with petrographic observations of olivine ± clinopyroxene ± oxide ±
323 plagioclase phenocryst assemblages in most Karacadağ phase lavas.

324 To explore the role of fractional crystallisation further we examined the ratios of
325 incompatible trace elements with similar bulk partition coefficients. Most group K1
326 and K2 lavas show no systematic variation in such ratios with changing MgO (Fig. 5).
327 There is relatively little variation of these ratios and almost complete overlap in the
328 ratios of groups K1 and K2 (Fig. 5). Therefore, we are confident that the model

329 generated from the alphaMELTS software captures the important features of
330 differentiation in these groups. However, there are two deviations from expected
331 behaviour. First, Sm/Zr shows a systematic change within group K1 (Fig. 5f). This
332 appears to be part of a progressive depletion in the middle (M-) and heavy rare earth
333 elements (HREE), relative to other elements with similar compatibility, with
334 decreasing MgO in K1 lavas. Since the absolute concentrations of REEs increase
335 with decreasing MgO (c.f. ytterbium in Fig. 2) we attribute this to the MREE and
336 HREE behaving slightly less incompatibly than normally expected during
337 crystallisation of the magma. Second, a small subset of group K1 has elevated K/La
338 and Ba/Yb at a particular value of MgO. Because Ba/Yb has previously been
339 proposed as a proxy for crustal contamination in the Karacadağ Volcanic Complex
340 we have identified this subset as Group K1a in Figures 3, 5 and 7. Their
341 development is discussed in the next section.

342 Group K3 compositions cannot be generated from a K2 parent, or vice versa.
343 Therefore, the K3 series records a distinct initial melt, while its major element
344 variations suggest differentiation under different conditions. In particular, garnet
345 crystallisation is required to suppress Al_2O_3 enrichment (with decreasing MgO) whilst
346 matching the other K3 major element characteristics. For the DK-26 parent
347 composition the optimum alphaMELTS model involves differentiation at 22.5 MPa,
348 initially of 5 % orthopyroxene with minor spinel followed by removal of an
349 assemblage comprising garnet, clinopyroxene and spinel. This achieves the
350 enrichment of K_2O and N_2O whilst suppressing Al_2O_3 and SiO_2 enrichment and also
351 depleting CaO in the melt (Fig. 7).

352 Ovabağ Phase lavas display restricted ranges in concentrations of all major
353 elements implying that fractional crystallisation played a limited role in the evolution
354 of these melts. Like group K2, the restricted variations within groups O1 and O2 can
355 be replicated by removal of less than 10% olivine, with minor spinel, from a parental

356 basalt with around 10 wt. % MgO. The similarity of group O3 to group K3 suggests
357 that these also differentiated at relatively high pressure.

358 **Crustal contamination**

359 Crustal contamination is known to have affected Neogene and Quaternary
360 magmatism throughout the Arabian Plate (Baker et al., 2000; Shaw et al., 2003;
361 Krienitz et al., 2009; Ma et al., 2011). For example, despite the absence of crustal
362 xenoliths or xenocrysts in the Miocene Siverek magmatism of the Karacadağ
363 Volcanic Complex, variations towards higher $^{87}\text{Sr}/^{86}\text{Sr}$, $\Delta 7/4$ and $\Delta 8/4$ and lower
364 $^{143}\text{Nd}/^{144}\text{Nd}$ demonstrate that some of those lavas interacted with the crust (Ekici et
365 al., 2012). Contamination was not a ubiquitous process, however, with only some
366 Siverek lavas displaying an isotopic signature of interaction with the crust. This
367 contamination had a negligible impact on incompatible trace element contents and
368 ratios, except for enriching Ba with respect to other elements. Selective Ba
369 enrichment most probably occurred because the contamination leverage for this
370 element – its concentration in the contaminant relative to the magma - was
371 significantly higher than that of other elements.

372 Concentrations of incompatible trace elements in Pliocene – Quaternary lavas are
373 similar to or greater than those in the most trace element enriched Siverek basalts.
374 Therefore, the same set of country rocks should exert even less contamination
375 leverage upon incompatible trace element concentrations in Karacadağ and Ovabağ
376 phase magma than was the case for Siverek. This is evaluated further in Fig. 5.
377 Rocks containing more than 8 wt. % MgO display the full range for most of the
378 incompatible trace element ratios and show no obvious correlations either within
379 particular groups or in the datasets as a whole. This observation suggests that
380 ranges for these ratios were present in the most primitive magma batches and that
381 crustal contamination had a negligible impact upon the trace element chemistry of
382 Mg-rich magma. The highest Ba/Yb ratios occur in the two most evolved members of

383 group K3 (Fig. 5). Yet, these same two samples show the lowest $^{87}\text{Sr}/^{86}\text{Sr}$, $\Delta 7/4$ and
384 $\Delta 8/4$, and highest $^{143}\text{Nd}/^{144}\text{Nd}$ observed for the Karacadağ and Ovabağ phases,
385 suggesting that a crustal influence was not required to generate the range of trace
386 element ratios observed in this magmatism.

387 Further insight comes from comparing the incompatible trace element ratios of
388 groups K1 and K2, which were shown to be related by fractional crystallisation
389 (previous section). The small subset of K1a lavas, with elevated Ba/Yb and K/La at a
390 given value of MgO, include sample DK-58 (Fig. 5), which possesses the most
391 extreme isotopic characteristics of all the Pliocene – Quaternary lavas (Fig. 6).
392 However, the changes to incompatible trace element ratios are small and not
393 systematic for all elements. For example, while group K1a lavas all have elevated
394 K/La and Ba/Yb (Fig. 5c), some do not show elevated K_2O or Ba at a given MgO
395 content, relative to the rest of group K1 (Fig. 3). Similarly, there are some other
396 group K1 lavas that have elevated K_2O and Ba but not elevated K/La and Ba/Yb.
397 There are negligible differences of the concentrations of most major and trace
398 elements in groups K1 and K1a. Only the alkali and alkaline earth elements show
399 systematic, although small, enrichments in the latter (Figs. 3 and 7). These,
400 apparently contradictory, observations probably reflect the low contamination
401 leverage of most crustal rocks on the trace element contents of magma from the
402 Karacadağ Volcanic Complex. Thus, while the K1a group suggests some magma –
403 crust interaction occurred, the restricted magnitude of variations suggest that most
404 trace element and isotopic ratios in Karacadağ and Ovabağ phase magma were not
405 modified significantly by crustal contamination.

406 Modelling the contamination that has occurred is hampered by the absence of data
407 for suitable crustal rocks for northern Arabia, a problem which has been recognised
408 by several studies (Shaw et al., 2003; Krienitz et al., 2006 and 2009; Ma et al.,
409 2011). To estimate the amount of melt – crust interaction we employed the approach
410 of Ekici et al. (2012) who used Sudanese lithologies to investigate crustal

411 contamination of Siverek plateau basalts. These offer a range of Sr, Nd and Pb
412 isotopic compositions with which to constrain the role of crustal rocks. In taking this
413 approach we are not trying to advocate any shared provenance between Sudanese
414 and Turkish basement but are testing the suitability of upper versus lower crustal
415 rocks as contaminants within the northern Arabian lithosphere. Since the K2 group
416 are parental to group K1 we used the K2 sample with the most elevated $^{143}\text{Nd}/^{144}\text{Nd}$
417 (KD-29) as the primitive magma in these models.

418 Contamination of a magma with the initial isotopic composition of DK-29 by lower
419 crust provides a good fit to Sr and Nd ratios of DK-58 with only a restricted amount of
420 differentiation ($F = 0.93$) for a relatively high ratio of assimilation to crystallisation ($r =$
421 0.75 ; model LC in Fig. 6). Contamination by upper crust does not produce such low
422 $^{143}\text{Nd}/^{144}\text{Nd}$ relative to $^{87}\text{Sr}/^{86}\text{Sr}$ as seen in DK-58. The lower crust model also
423 provides a more suitable fit to the displacement of DK-58 in Pb isotope space.
424 However, the amount of contaminant required to produce the Sr and Nd isotopic
425 variation would, in most cases, lead to substantially more extreme Pb isotopic ratios
426 than observed in DK-58. This may be because the parental melt was significantly
427 richer in Pb than DK-29 or the crust beneath Karacadağ was able to exert
428 considerably less Pb isotopic leverage than these models suggest. In either case,
429 the amount of contamination suggested by Pb is substantially less than estimated
430 from $^{87}\text{Sr}/^{86}\text{Sr}$ and $^{143}\text{Nd}/^{144}\text{Nd}$ for DK-58. Therefore, the Sr and Nd isotope data
431 provide an upper limit for contamination of 5% and suggests most batches of magma
432 experienced substantially less contamination than this.

433 **Composition of mantle sources**

434 Crustal contamination introduced little isotopic and trace element heterogeneity into
435 magma of the Karacadağ and Ovabağ phases. Therefore, most of the variation in
436 these lavas must have existed in their parental magmas. Previous studies of
437 northern Arabian Plate volcanism have advocated peridotitic sources with elemental

438 concentrations resembling primitive mantle (Shaw et al., 2003; Ekici et al., 2012). In
439 addition, Ma et al. (2011) invoked garnet-bearing hornblendite veins to explain the
440 incompatible trace element characteristics of low-silica lavas from the northern Dead
441 Sea Fault. In this section, we shall explore the origin of the variation in the source of
442 Karacadağ Volcanic Complex lavas. Since group K1 experienced greater
443 differentiation than the remaining groups we shall exclude these whilst constraining
444 the trace element characteristics of sources beneath the north Arabian Plate.
445 However, we shall include relevant K1 data when using isotopic ratios to place
446 further constraints upon those sources.

447 Ovabağ data show how the rare earth element systematics of the Karacadağ
448 Volcanic Complex lavas can be reconciled with fractional, non-modal melting of
449 peridotite with element concentrations resembling primitive mantle, with or without a
450 small amount of MREE enrichment (Shaw et al., 2003; Ekici et al., 2012). Groups O2
451 through O1 to O3 form a shallow, positive array in Dy/Yb versus La/Yb space (Fig.
452 8a). The low Dy/Yb ratios in the group O2 lavas coincide with the spinel lherzolite
453 melting model suggesting low degrees of melting (2 to 3 %) of a relatively shallow
454 source. Groups O1 and O3 form a tight cluster trending from O2 values towards a
455 restricted range of compositions with high Dy/Yb and La/Yb, which would represent
456 low degree (< 1.5 %) partial melting of a garnet lherzolite. Therefore, groups O2 and
457 O3 represent mixtures of melt from primitive spinel lherzolite with progressively
458 greater amounts of melt derived from below the spinel - garnet transition. The tight
459 array suggests little variation in the degree of partial melting in the shallow and deep
460 sources. The greater prominence of low degrees of partial melting implied for the
461 group O3 lavas is also consistent with their higher trace element contents (Fig. 3).
462 Groups K2 and K3 can be interpreted in a similar way but are displaced from the
463 Ovabağ array to intersect the modelled melting curves at higher degrees of melting
464 (Fig. 8a). In addition, the more elevated Dy/Yb values in group K3 also indicate a
465 greater relative contribution from garnet lherzolite.

466 Models invoking primitive mantle concentrations of REEs provide valuable
467 information on the relative contributions from different depths during polybaric
468 melting of the mantle. But Karacadağ Volcanic Complex lavas show fractionation of
469 large ion lithophile elements from both the rare earth elements and high field
470 strength elements, which cannot be produced by melts of primitive spinel- and
471 garnet-lherzolite alone (Fig. 8c). These fractionations also preclude an origin
472 involving only a primitive mantle and hornblendite veins as proposed by Ma et al.
473 (2011), which cannot generate the $(K/La)_n$ values greater than one that are common
474 to groups K2, O1 and O2. The low K/La and K/Nb ratios of group K3 lavas could be
475 interpreted as reflecting derivation from a source containing hornblendite (Fig. 8c)
476 but their elevated and variable Dy/Yb ratios are not consistent with this origin (Fig.
477 8a). Furthermore, low Sm/Zr ratios suggest a limited or non-existent role for this
478 lithology in the genesis of all Karacadağ Volcanic Complex lavas (Fig. 8d).

479 Incompatible trace element ratios of Karacadağ and Ovabağ lavas are not consistent
480 with derivation from a carbonated mantle (Nelson et al., 1988; Blundy and Dalton,
481 2000; Dixon et al., 2008; Sisson et al., 2009). They display low Ba/Th and elevated
482 Nb/La, with the most silica-poor (Mg-rich) liquids possessing the lowest La/Nb (Fig.
483 5e), and Zr depletion is negligible (Fig. 4 and Fig. 5f). These signatures also contrast
484 with those proposed for carbonated mantle in the northern Arabian Plate (Shaw et
485 al., 2007). Therefore, in an attempt to reproduce the incompatible trace element
486 variation we modelled melting of hydrous garnet lherzolite (Fig. 9). Fractional, non-
487 modal melting was modelled for two sources. First, we explored the amphibole-
488 bearing source and melting proportions given by Ma et al. (2011). The second model
489 was a phlogopite-garnet peridotite of Sisson et al. (2009) using partition coefficients
490 from Sisson et al. (2009) and Adam and Green (2011). Neither model, by itself,
491 reproduces the range of compositions observed in the Karacadağ Volcanic Complex
492 lavas or in the different groups that we have identified. However, mixtures of melts
493 from phlogopite-bearing mantle and anhydrous sources with a small enrichment of

494 the most incompatible elements can achieve many of the key characteristics (Sisson
495 et al., 2009).

496 Mixtures between melt from an amphibole-garnet lherzolite and anhydrous, enriched
497 (garnet- or spinel-) lherzolite cannot reproduce the low Ba/La and Ba/Yb and
498 relatively high Zr/Nb ratios seen in many of the lavas from the Karacadağ and
499 Ovabağ phases (Fig. 9a, c and d). This source does, however, provide a particularly
500 good fit to Jordanian Harrat Ash Shaam lavas (Shaw et al., 2007) for all ratios except
501 Rb/Ba (see below). This suggests that the trace element enrichment of magmatism
502 close to the Syrian – Jordanian border may be due to the presence of significant
503 amounts of amphibole in the mantle (Fig. 9a, c and d) but amphibole does not
504 appear to be an important component in the mantle beneath Karacadağ.

505 Although melts from phlogopite-garnet lherzolite are not suitable as sole sources
506 they do display some of the key trace element features that characterise the
507 Karacadağ and Ovabağ lavas. Elevated Zr/Nb at low K/La, and low Ba/Yb and Ba/La
508 are all predicted for melts derived from this source (Fig. 9a,c and d). Since REE
509 systematics suggest derivation over a range of depths (Fig. 8a) we suggest that the
510 Pliocene to Quaternary Karacadağ Volcanic Complex lavas were derived from
511 mixtures of melt derived from three sources: phlogopite-bearing garnet lherzolite,
512 enriched garnet lherzolite and enriched spinel lherzolite. No simple binary mixtures
513 can reproduce the entire data array. However, mixtures of 1.5 to 5 % partial melts of
514 phlogopite-garnet-peridotite with low degree (< 1 %) partial melts from anhydrous
515 lherzolite reproduce most of the key features (Fig. 9a,c and d). The major problem
516 comes in reproducing the low Rb/Ba ratios of the northern Arabian intra-plate
517 magmatic suites (Fig. 9). We have tried various manipulations of the models to
518 achieve low Rb/Ba, particularly coupled to elevated La/Yb (Fig. 9b) whilst
519 maintaining the fits achieved for other ratios. We speculate that the most likely
520 solution is a relatively high partition coefficient for Rb in phlogopite (e.g. $D_{\text{Rb}}^{\text{phlog}} > 8$),
521 which is not unreasonable (Ionov et al., 1997).

522 Thus, we propose that most Karacadağ Volcanic Complex lavas originated as
523 mixtures of (i) melt derived from enriched, anhydrous lherzolite over a range of
524 depths, with (ii) melt derived from phlogopite-bearing garnet lherzolite. While lavas
525 from Harrat Ash Shaam or the northern Dead Sea Fault appear to record evidence
526 for amphibole in their sources (Shaw et al., 2003; Ma et al., 2011) there is little
527 evidence to support its involvement at Karacadağ (Figs. 8 and 9). Having invoked
528 three-component mixing in the mantle, it is difficult to also place more quantitative
529 constraints on the degree of partial melting. However, using the REEs, which should
530 be modified by metasomatism in a relatively systematic fashion, suggests that the
531 Pliocene to Quaternary Karacadağ Volcanic Complex lavas formed through small
532 degrees of partial melting similar to those calculated for other parts of the northern
533 Arabian Plate (Fig. 7a).

534 **Origin of mantle sources**

535 Prior studies have identified a number of potential mantle sources beneath the
536 Arabian Plate that could contribute to intraplate magmatism. These include
537 lithospheric mantle, variably enriched by metasomatism or metasomatic phases, the
538 convecting upper mantle and outflow of mantle derived from the Afar triple junction
539 (Çapan et al., 1987; Pearce et al., 1990; Camp and Roobol, 1992; Bertrand et al.,
540 2003; Shaw et al., 2003; Şen et al., 2004; Weinstein et al., 2006; Krienitz et al.,
541 2006, 2007 and 2009; Lustrino et al., 2010; Ma et al., 2011; Ekici et al., 2012). Most
542 of these studies have identified multiple components at any one site. In this section
543 we shall evaluate the isotopic ratios of Pliocene to Quaternary magmatism in the
544 Karacadağ Volcanic Complex relative to other locations in the northern Arabian Plate
545 and the implications for mantle sources throughout this area.

546 Karacadağ Volcanic Complex lavas lack $^{206}\text{Pb}/^{204}\text{Pb}$ in excess of 19.1, in contrast to
547 the Harrat Ash Shaam, Dead Sea Fault and northern Syria, where a high $^{206}\text{Pb}/^{204}\text{Pb}$
548 component has been invoked (Bertrand et al., 2003; Krienitz et al., 2009; Ma et al.,

549 2011). This component is most conspicuous in high- $^{206}\text{Pb}/^{204}\text{Pb}$ lavas from Karasu
550 Valley and Dead Sea Fault from which a $^{206}\text{Pb}/^{204}\text{Pb}$ ratio greater than 19.5, with
551 $^{207}\text{Pb}/^{204}\text{Pb}$ and $^{208}\text{Pb}/^{204}\text{Pb}$ ratios close to the Northern Hemisphere Reference Line,
552 can be inferred (Fig. 6c and d). This high- $^{206}\text{Pb}/^{204}\text{Pb}$ component was attributed to
553 the Afar plume by Krienitz et al. (2009) although others have suggested it was an
554 older, lithospheric source (Bertrand et al., 2003). A clear distinction between the $\Delta 8/4$
555 values of Afar plume magmatism and Arabian intraplate lavas, including the
556 Karacadağ Volcanic Complex, precludes involvement of Afar plume in magmatism of
557 the northernmost Arabian Plate (Fig. 6d). Regardless of its origin, however, the high-
558 $^{206}\text{Pb}/^{204}\text{Pb}$ component has not made a significant contribution to Karacadağ
559 Volcanic Complex magmatism.

560 A group K3 lava displays the lowest $^{207}\text{Pb}/^{204}\text{Pb}$ and $^{208}\text{Pb}/^{204}\text{Pb}$ for a given
561 $^{206}\text{Pb}/^{204}\text{Pb}$ of any sample from the Karacadağ Volcanic Complex. The Sr and Nd
562 isotopic ratios of this sample (DK-25) are similar to low- $^{206}\text{Pb}/^{204}\text{Pb}$ samples from
563 Harrat Ash Shaam and northern Syria (Bertrand et al., 2003; Shaw et al., 2003;
564 Krienitz et al., 2009). Therefore, we interpret this as an endmember that is common
565 to much of the intraplate magmatism across northern Arabia and, as previously
566 suggested by Shaw et al. (2003) and Krienitz et al. (2009), the low $^{206}\text{Pb}/^{204}\text{Pb}$, $\Delta 7/4$,
567 $\Delta 8/4$ and $^{87}\text{Sr}/^{86}\text{Sr}$ and high $^{143}\text{Nd}/^{144}\text{Nd}$ indicate that this is probably depleted upper
568 mantle. Rare earth element systematics demonstrate that group K3 lavas contain a
569 relatively large contribution from the garnet stability field and so the distinctive K3
570 isotopic composition could reflect melt derived from either lithospheric or
571 asthenospheric mantle. Workman and Hart (2005) characterised the long-known
572 range of compositions in the depleted mantle as a spectrum spanning enriched (E-
573 DMM) to depleted (D-DMM) end-members. The isotopic ratios of DK-25 are very
574 similar to those of E-DMM, which is likely to represent the most fusible component of
575 the convecting mantle. Therefore, the K3 composition might represent small degree
576 melts from the convecting mantle, in which phlogopite can be stable (Luth, 2003).

577 Alternatively, such melts may metasomatise the base of the lithospheric mantle
578 (McKenzie, 1989) providing a hydrated lherzolite source resembling E-DMM that
579 could contribute to magmatism generated throughout the region. Kovács et al.
580 (2012) suggest that phlogopite would be the primary hydrous phase in peridotite at
581 pressures greater than 3 GPa although the presence of this and alternative water-
582 bearing phases at lower pressures, principally the amphibole pargasite, is also
583 dependent on the bulk composition and the absolute water content of the mantle.

584 Incompatible element systematics indicate that group K1 and K2 lavas contain
585 greater contributions from shallower mantle (Fig. 8 and 9). Melting at shallow levels
586 could occur if asthenosphere upwells sufficiently to melt to higher degrees, so
587 allowing increased dilution of the E-DMM component by melts from more refractory
588 parts of the mantle (Elliott et al., 1991). However, this is not consistent with the
589 higher $^{87}\text{Sr}/^{86}\text{Sr}$ and lower $^{143}\text{Nd}/^{144}\text{Nd}$ of the group K1 and K2 lavas (Fig. 6). In
590 addition, large degrees of asthenospheric upwelling would be difficult to reconcile
591 with limited or highly localised extensional tectonics during magmatism at Mt.
592 Karacadağ (Adiyaman and Chorowicz, 2002). Therefore, we suggest that the lavas
593 of groups K1 and K2 are dominated by melts derived from enriched parts of the
594 shallow lithospheric mantle. The enriched, lithospheric source possesses $^{87}\text{Sr}/^{86}\text{Sr} \sim$
595 0.70370 and $^{143}\text{Nd}/^{144}\text{Nd} \sim 0.51286$. Pb isotope ratios are more difficult to constrain
596 due to the possible influence of crustal contamination. However, the enriched
597 lithosphere is likely to have slightly lower $^{206}\text{Pb}/^{204}\text{Pb}$ than the depleted component
598 and slightly more elevated $\Delta 7/4$ and $\Delta 8/4$ (Fig. 6).

599 Shaw et al. (2003) concluded that the Jordanian part of the Harrat Ash Shaam was
600 also derived from mixtures of deep, depleted and shallow, enriched mantle. Despite
601 the evidence for differences in the nature of hydrous phases between Karacadağ
602 and Harrat Ash Shaam (Fig. 9), the isotopic data indicate that the two volcanic
603 regions are probably derived from similar types of mantle.

604 Magma transport through the crust at Mt. Karacadağ

605 The thickness of individual lava flows was not measured as part of this study so we
606 cannot quantify the relative volumes of magma generated by different parts of the
607 Karacadağ volcano. However, most lavas initially flowed laterally from the loci of
608 eruption therefore some constraints can be obtained by observing where each group
609 predominates along the ridge crest. We combine this information with constraints
610 obtained from fractional crystallisation models to interpret magma transport during
611 the Karacadağ Phase of magmatism. Group K1 lavas were mainly erupted on and
612 around the northern summit of Mt. Karacadağ but were much less abundant on the
613 central and southern summits (Fig. 1b). Lavas of group K2, in contrast, are present
614 along the length of the ridge. This suggests that the magmatic plumbing at the
615 northern end of the volcano was conducive to eruption of magma that had
616 differentiated more extensively.

617 Late Cenozoic stress in the northern Arabian Plate was produced by its collision with
618 Anatolia. The resultant westward escape of Anatolia, accommodated in southern
619 Turkey along the East Anatolian Fault (Fig. 1a), has caused different types of strain
620 throughout northern Arabia. Adiyaman and Chorowicz (2002) attributed the Mt
621 Karacadağ fissure to far-field, east – west tension that diminished towards the south,
622 distal to the collision. If this tensional stress diminished southward along the
623 Karacadağ fissure then the northern part of the volcano could have provided a larger
624 accommodation volume in the crust into which more magma could be emplaced.
625 This, in turn, would supply more heat into surrounding crustal rocks, which would
626 account for the northern K1 group providing the few examples where we observed
627 evidence for crustal contamination. A differentiation pressure of 5 MPa, as
628 determined for groups K1 and K2 from the alphaMELTS models, indicates
629 crystallisation close to the postulated upper to lower crust transition of 19 km (Nasir
630 and Safarjalani, 2000). This depth has also been proposed as the transition from
631 brittle to ductile behaviour of crust in northern Arabia (Adiyaman and Chorowicz,

632 2002). Thus, we suggest that differentiation could proceed further at the northern
633 end of Mt. Karacadağ as a result of relatively large volumes of magma ponding close
634 to the petrological and rheological boundary between upper and lower crust (Fig. 10).
635 Elsewhere along the fissure, the cooler crust would have impeded development of
636 extensive storage zones and magma experienced less differentiation, resulting in the
637 more primitive K2 lava flows.

638 Group K3 has a restricted distribution on the Mt. Karacadağ ridge, being the
639 predominant lava type of the central summit with a minor presence on the northern
640 summit (Fig. 1b). Most of these have elevated MgO contents and the fractional
641 crystallisation models reflect very restricted amounts of differentiation. The distinctive
642 chemistry of this group, however, does require differentiation high at pressure (Fig.
643 7) and it is tempting to equate the modelled pressure of 22.5 MPa with the 80 km
644 depth estimated for the lithosphere – asthenosphere transition zone in northern
645 Arabia (McGuire and Bohannon, 1989; Nasir and Safarjalani, 2000). The lack of
646 evidence for low pressure crystallisation suggests that, subsequent to fractionation
647 close to the base of the lithosphere, group K3 magmas experienced negligible further
648 differentiation before eruption.

649

CONCLUSIONS

650 Mt. Karacadağ is the most conspicuous feature of the Karacadağ Volcanic Complex,
651 forming an elongate shield volcano that has produced lateral lava flows from its north
652 – south oriented axis. This form suggests that lithospheric tension localised
653 magmatism during the Pliocene and Quaternary. East-west tension in this part of the
654 Arabian Plate was the result of local stress due to the initiation of the Eastern
655 Anatolian Fault (Adiyaman and Chorowicz, 2002). Late in the history of the
656 Karacadağ Volcanic Complex magmatism migrated to Ovabağ, where lavas were
657 erupted from monogenetic cones and represent melting and emplacement in the
658 absence of significant lithospheric tension.

659 Previously, we interpret the earlier, Miocene phase of magmatism as the result of
660 melting when mantle upwelled beneath a lithospheric weak-spot as the Arabian Plate
661 migrated north and east during the Cenozoic (Ekici et al., 2012). The Karacadağ and
662 Ovabağ phases may represent renewed melting through this process although
663 localised tectonic processes served to focus magmatism. In the case of Mt.
664 Karacadağ, localised extension may also have played a role in causing melting but
665 there is restricted geological evidence at the surface to support this. Isotopic data
666 indicate that mantle derived from the Afar plume was not involved in genesis of
667 Karacadağ Volcanic Complex lavas.

668 Trace element systematics of the Karacadağ Volcanic Complex lavas were
669 influenced by the presence or absence of small quantities (< 2 %) of phlogopite in
670 the mantle. The lavas do not display evidence for derivation exclusively from
671 amphibole veins in the mantle as proposed for magmatism from Al Ghab volcanic
672 field in the Dead Sea Fault (Ma et al., 2011) or for melting of carbonated mantle
673 (Shaw et al., 2007).

674 Trace element and isotopic ratios of groups K3 and O3 lavas are distinct in their low
675 contents of silica and Al_2O_3 and their elevated TiO_2 and incompatible element
676 contents, relative to other groups. Depletion in potassium, relative to other elements
677 of similar compatibilities, coupled with the absence of extreme Ba enrichment
678 indicates that phlogopite was present in the source of these lavas. These groups
679 display trace element ratios which indicate a relatively large contribution from garnet-
680 facies lherzolite. Isotopic characteristics of the lavas resemble the most fusible part
681 of the convecting upper mantle but such a signature could also be transferred to the
682 base of the lithospheric mantle by migration of low degree melts. This component is
683 common to other volcanic fields across northern Arabia. Once generated, K3 and O3
684 magmas experienced minor differentiation near the base of the lithosphere prior to
685 eruption.

686 Groups K2, O1 and O2 represent melting across a range of depths but with a greater
687 contribution from spinel-lherzolite in the lithospheric mantle than in the K3 and O3
688 groups. These groups also have more elevated $^{87}\text{Sr}/^{86}\text{Sr}$ and Pb isotopic ratios and
689 lower $^{143}\text{Nd}/^{144}\text{Nd}$ than groups K3 and O3. Group K2 were produced along the length
690 of the 30 km Karacadağ fissure and crystallised limited amounts of olivine close to
691 the transition between upper and lower crust. At the northern end of the Mt.
692 Karacadağ volcano more protracted differentiation of K2 parental magma at the
693 upper – lower crust transition produced magma of group K1. This and the greater
694 amount of crustal contamination observed to the north resulted from greater stress in
695 the crust at the Anatolian end of the Karacadağ fissure. Lavas from groups O1 and
696 O2 show similar trace element and isotopic systematics to Group K2 suggesting that
697 mantle sources sampled by the Karacadağ phase could be generated in the absence
698 of significant lithospheric extension.

699

ACKNOWLEDGEMENTS

700 Taner Ekici acknowledges financial support from TUBITAK (Project No. 107Y025) to
701 conduct fieldwork and analytical work. Mehmet Ülkü of MTA Diyarbakır supported
702 fieldwork in SE Turkey. Colin Macpherson is grateful to Durham University for a
703 period of research leave. We thank Mark Allen and Iain Neill for discussion.
704 Comments by Christoph Beier and an anonymous reviewer were very constructive
705 and led to significant improvements in this manuscript, as was the editorial input from
706 Richard Price.

707

REFERENCES

708 Adam, J. & Green, T. (2006). Trace element partitioning between mica- and
709 amphibole-bearing garnet lherzolite and anhydrous basanitic melt: 2. Tasmanian
710 Cainozoic basalts and the origins of intraplate basaltic magmas. *Contribution to*
711 *Mineralogy and Petrology* **161**, 883-899, doi:10.1007/s00410-010-0570-7.

- 712 Adiyaman, Ö. & Chorowicz, J. (2002). Late Cenozoic tectonics and volcanism in the
713 northwestern corner of the Arabian plate: a consequence of the strike-slip Dead Sea
714 fault zone and the lateral escape of Anatolia. *Journal of Volcanology and Geothermal*
715 *Research* **117**, 327-345.
- 716 Allen, M., Jackson, J. & Walker, R. (2004). Late Cenozoic reorganization of the
717 Arabia-Eurasia collision and the comparison of short-term and long term deformation
718 rates. *Tectonics* **23**, TC2008, doi: 10.1029/2003TC001530.
- 719 Baker, J.A., Macpherson, C.G., Menzies, M.A., Thirlwall, M.F., Al-Kadasi, M. &
720 Matthey, D.P. (2000). Resolving crustal and mantle contributions to continental flood
721 volcanism, Yemen: Constraints from mineral oxygen isotope data. *Journal of*
722 *Petrology* **41**, 1805-1820.
- 723 Bertrand, H., Chazot, G., Blichert-Toft, J. & Thoral, S. (2003). Implications of
724 widespread high- μ volcanism on the Arabian Plate for Afar mantle plume and
725 lithosphere composition. *Chemical Geology* **198**, 47-61.
- 726 Blundy, J. & Dalton, J. (2000). Experimental comparison of trace element partitioning
727 between clinopyroxene and melt in carbonate and silicate systems, and implications
728 for mantle metasomatism. *Contributions to Mineralogy and Petrology* **139**, 356-371.
- 729 Brigland, D., Demir, T., Seyrek, A., Pringle, M., Westaway, R., Beck, A., Yurtmen, S.
730 & Rowbotham, G. (2007). Dating Quaternary volcanism and incision by the River
731 Tigris at Diyarbakır, SE Turkey. *Journal of Quaternary Science* **21**, 437-455, doi:
732 10.1002/jqs.1074.
- 733 Camp, V.E. & Roobol, M.J. (1992). Upwelling Asthenosphere beneath western
734 Arabia and its regional implications. *Journal of Geophysical Research* **97**, 15,255-
735 271.

- 736 Chiaradia, M., Müntener, O. & Beate, B. (2011). Enriched basaltic andesites from
737 mid-crustal fractional crystallization, recharge, and assimilation (Pilavo volcano,
738 Western Cordillera of Ecuador). *Journal of Petrology* **52**, 1107-1141, doi:
739 10.1093/petrology/egr020.
- 740 Çapan, U.Z., Vidal, P. & Contagrel, L.M. (1987). K-Ar, Nd, Sr and Pb isotopic study
741 of Quaternary volcanism in Karasu Valley (Hatay), N end of Dead Sea rift zone in SE
742 Turkey. *Yerbilimleri* **14**, 165-178.
- 743 Davidson, J.P. & Wilson, I.R. (1989). Evolution of an alkali basalt-trachyte suite from
744 Jebel Marra volcano, Sudan, through assimilation and fractional crystallisation. *Earth
745 and Planetary Science Letters* **95**, 141-160.
- 746 Demir, T., Westaway, R., Brigland, D., Pringle, M., Yurtmen, S., Beck, A. &
747 Rowbotham, G. (2007). Ar-Ar dating of late Cenozoic basaltic volcanism in northern
748 Syria: Implications for the history of incision by the River Euphrates and uplift of the
749 northern Arabian Platform. *Tectonics* **26**, TC3012, doi:10.1029/2006TC001959.
- 750 Deniel, C., Vidal, P., Coulon, C., Vellutini, P.J. & Piquet, P. (1994). Temporal
751 evolution of mantle sources during continental rifting: the volcanism of Djibouti (Afar).
752 *Journal of Geophysical Research* **99**, 2853-2869.
- 753 DePaolo, D.J., 1981. Trace element and isotopic effects of combined wallrock
754 assimilation and fractional crystallisation. *Earth and Planetary Science Letters* **53**,
755 189–202.
- 756 Dixon, J.E., Clague, D.A., Cousens, B., Monsalve, M.L. & Uhl, J. (2008). Carbonatite
757 and silicate melt metasomatism of the mantle surrounding the Hawaiian plume:
758 evidence from volatiles, trace elements, and radiogenic isotopes. *Geochemistry,
759 Geophysics, Geosystems* **9**, Q09005.

- 760 Dungan, M.A. & Rhodes, M.J. (1978). Residual glasses and melt inclusions in
761 basalts from DSDP legs 45 and 46: evidence for magma mixing. *Contributions to*
762 *Mineralogy and Petrology* **67**, 417-431.
- 763 Ekici, T., Macpherson, C.G. & Otlu, N. (2012). Polybaric melting of a single mantle
764 source during the Neogene Siverek phase of the Karacadağ Volcanic Complex, SE
765 Turkey. *Lithos* 146-147, 152-163.
- 766 Ekici, T., Macpherson, C.G. & Otlu, N. (submitted). Intraplate magmatism generated
767 by shear-induced melting during Arabian plate motion: Evidence from Volcanic
768 Complex, southeast Turkey. Submitted to *Journal of the Geological Society of*
769 *London*.
- 770 Elliott, T.R., Hawkesworth, C.J., & Gronvold, K. (1991). Dynamic melting of the
771 Iceland plume. *Nature* **351**, 201-206.
- 772 El-Isa, Z., Mechie, J. & Prodehl, C. (1987a). Shear velocity structure of Jordan from
773 explosion seismic data. *Geophysical Journal of the Royal Astronomical Society* **90**,
774 265-281.
- 775 El-Isa, Z., Mechie, J., Prodehl, C., Makris, J. & Rihm, R. (1987b). A crustal structure
776 study of Jordan derived from seismic refraction data. *Tectonophysics* **138**, 235-253.
- 777 Ercan, T., Fujitani, T., Matsuda, J.I., Notsu, K., Tokel, S. & ve Ul, T. (1990). Doğu ve
778 Güneydoğu Anadolu Neojen-Kuvaterner Volkanitlerine ilişkin yeni jeokimyasal,
779 radyometrik ve izotopik verilerin yorumu. *MTA Dergisi* **110**, 143-164.
- 780 Gürsoy, H., Tatar, O., Piper, J.D.A., Koçbulut, F. & Mesci, B.L. (2009).
781 Paleomagnetic study of Tertiary volcanic domains in Southern Turkey and Neogene
782 anticlockwise rotation of the Arabian Plate. *Tectonophysics* **465**, 114-127,
783 doi:10.1016/j.tecto.2008.11.001.

- 784 Hart, S.R. (1984). A large-scale isotope anomaly in the Southern Hemisphere
785 mantle. *Nature* **309**, 753-757.
- 786 Ilani, S., Harlavan, Y., Tarawneh, K., Rabba, I., Weinberger, R., Ibrahim, K., Peltz,
787 S. & Steinitz, G. (2001). New K-Ar ages of basalts from the Harrat Ash Shaam
788 volcanic field in Jordan: Implications for the span and duration of the upper-mantle
789 upwelling beneath the western Arabian plate. *Geology* **29**, 171-174.
- 790 Ionov, D.A., Griffin, W.L. & O'Reilly, S.Y. (1997) Volatile-bearing minerals and
791 lithophile elements in the upper mantle. *Chemical Geology* **141**, 153-184.
- 792 Keskin, M. (2003). Magma generation by slab steepening and breakoff beneath a
793 subduction-accretion complex: An alternative model for collision-related volcanism in
794 Eastern Anatolia, Turkey. *Geophysical Research Letters* **30**, 8046, doi:10,
795 1029/2003GL018019.
- 796 Krienitz, M.S., Haase, K.M., Mezger, K., Eckardt, V. & Shaikh-Mashail, M.A. (2006).
797 Magma genesis and crustal contamination of continental intraplate lavas in
798 Northwestern Syria. *Contributions to Mineralogy and Petrology* **151**, 698-716,
799 doi:10.1007/s00410-006-0088-1.
- 800 Krienitz, M.S., Haase, K.M., Mezger, K. & Shaikh-Mashail, M.A. (2007). Magma
801 genesis and mantle dynamics at Harrat Ash Shamah volcanic field (Southern Syria).
802 *Journal of Petrology* **48**, 1513-1542, doi:10.1093/petrology/egm028.
- 803 Krienitz, M.S., Haase, K.M., Mezger, K., Van den Bogard, P., Thiemann, V. &
804 Shaikh-Mashail, M.A. (2009) Tectonics events, continental intraplate volcanism, and
805 mantle plume activity in northern Arabia: Constraints from geochemistry and Ar-Ar
806 dating of Syrian lavas. *Geochemistry Geophysics Geosystems* **10**, Q04008,
807 doi:10.1029/2008GC002254.

- 808 Kovács, I., Green, D.H., Rosenthal, A., Hermann, J., O'Neil, H.S., Hibberson, W.O. &
809 Udvardi, B. (2012) An experimental study of water in nominally anhydrous minerals
810 in the upper mantle near the water-saturated solidus. *Journal of Petrology* **53**, 2067-
811 2093.
- 812 Lustrino, M., Keskin, M., Mattioli, M. & Kavan, O. (2012) Heterogeneous mantle
813 sources feeding the volcanic activity of Mt. Karacadağ. *Journal of Asian Earth*
814 *Sciences* **46**, 120-139.
- 815 Lustrino, M., Keskin, M., Mattioli, M., Lebedev, V.A., Chugaev, A., Sharkov, E. &
816 Kavak, O. (2010). Early activity of the largest Cenozoic shield volcano in the circum-
817 Mediterranean area: Mt. Karacadağ, SE Turkey. *European Journal of Mineralogy* **22**,
818 343-362, doi:10.1127/0935-1221/2010/0022-2024.
- 819 Luth, R.W. (2003). Mantle volatiles – distribution and consequences, pp. 319-361. In
820 *The Mantle and Core* (ed. R.W. Carlson) Vol 2 *Treatise on Geochemistry* (eds. H.D.
821 Holland & K.K. Turekian), Elsevier-Pergamon, Oxford.
- 822 Ma, G.S.-K., Malpas, J., Xenophontos, C. & Chan, G.H.-N. (2011). Petrogenesis of
823 latest Miocene-Quaternary continental intraplate volcanism along the northern Dead
824 Sea Fault system (Al Ghab – Homs volcanic field), western Syria: Evidence for
825 lithosphere – asthenosphere interaction. *Journal of Petrology* **52**, 401-430,
826 doi:10.1093/petrology/egq085.
- 827 McDonough, W.F. & Sun, S.S. (1995). The composition of the Earth. *Chemical*
828 *Geology* **120**, p. 223-253.
- 829 McGuire, A.V. & Bohannon, R.G. (1989). Timing of mantle upwelling: Evidence for a
830 passive origin for the Red Sea Rift. *Journal of Geophysical Research* **94**, 1677-1682.
- 831 McKenzie, D. (1989). Some remarks on the movement of small melt fractions in the
832 mantle. *Earth and Planetary Science Letters* **95**, 53-72.

- 833 Nasir, S. (1992). The lithosphere beneath the northwestern part of the Arabian plate
834 (Jordan): evidence from xenoliths and geophysics. *Tectonophysics* **201**, 357-370.
- 835 Nasir, S. & Safarjalani, A. (2000). Lithospheric petrology beneath the northern part of
836 the Arabian Plate in Syria: evidence from xenoliths in alkali basalts. *Journal of*
837 *African Earth Sciences* **30**, 149-168.
- 838 Nelson, S.T. & Montana, A. (1992). Sieve-textured plagioclase in volcanic rocks
839 produced by rapid decompression. *American Mineralogist* **77**, 1242-1249.
- 840 Nelson, D.R., Chivas, A.R., Chappell, B.W. & McCulloch, M.T. (1988). Geochemical
841 and isotopic systematics in carbonatites and implications for the evolution of ocean-
842 island sources. *Geochimica et Cosmochimica Acta* **52**, 1-17.
- 843 Pearce, J.A., Bender, J.F., DeLong, S.E., Kidd, W.S.F., Low, P.J., Güner, Y.,
844 Şaroğlu, F., Yılmaz, Y., Moorbath, S. & Mitchell, J.G. (1990). Genesis of collision
845 volcanism in eastern Anatolia, Turkey. *Journal of Volcanology and Geothermal*
846 *Research* **44**, 184-229.
- 847 Pik, R., Deniel, C., Coulon., Yirgu, G. & Marty, B. (1999). Isotopic and trace element
848 signatures of Ethiopian flood basalts: evidence for plume-lithosphere interactions
849 from Na/Ti and rare earth element ratios. *Journal of Geophysical Research* **104**,
850 2817-2829.
- 851 Robertson, A.H.F. (2000). Mesozoic-Tertiary tectonic-sedimentary evolution of a
852 south Tethyan oceanic basin and its margins in southern Turkey In: Bozkurt, E.,
853 Winchester, J.A. & Piper, J.D.A. (eds), *Tectonics and Magmatism in Turkey and the*
854 *Surrounding Area. Geological Society of London Special Publications* **173**, 97-138.
- 855 Şen, P.A., Temel, A. & Gourgau, A. (2004). Petrogenetic modelling of Quaternary
856 post-collisional volcanism: A case study of central and eastern Anatolia. *Geological*
857 *Magazine* **141**, 81-98, doi: 10.1017/S0016756803008550.

- 858 Şengör, A.M.C., Özeren, M.S., Keskin, M., Sakıncı, M., Özbakır, A.D. & Kayan, İ.
859 (2008). Eastern Turkish high plateau as a small Turkish-type orogen: Implications for
860 post-collisional crust forming processes in Turkish-type orogens. *Earth Science*
861 *Reviews* **90**, 1-48, doi:10.1016/j.earscirev.2008.05.002.
- 862 Shaw, J.E., Baker, J.A., Menzies, M.A., Thirlwall, M.F. & Ibrahim, K.M. (2003).
863 Petrogenesis of the largest intraplate volcanic field on the Arabian Plate (Jordan): a
864 mixed Lithosphere-Asthenosphere source activated by Lithospheric extension.
865 *Journal of Petrology* **44**, 1657-1679, doi:10.1093/petrology/egg052.
- 866 Shaw, J.E., Baker, J.A., Kent, A.J.R., Ibrahim, K.M., & Menzies, M.A. (2003). The
867 geochemistry of the Arabian lithospheric mantle – a source for intraplate volcanism?
868 *Journal of Petrology* **48**, 1495-1512.
- 869 Sisson, T.W., Kimura, J.-I. & Coombs, M.L. (2009). Basanite-nephelinite suite from
870 early Kilauea: carbonated melts of phlogopite-garnet peridotite at Hawaii's leading
871 magmatic edge. *Contributions to Mineralogy and Petrology* **158**, 803-829.
872 doi:10.1007/s00410-009-0411-8.
- 873 Smith, P.M. & Asimow, P.D. (2005). Adibat_1ph: A new public front-end to the
874 MELTS, pMELTS, and pHMELTS models. *Geochemistry, Geophysics, Geosystems*
875 **6** Q02004. doi: 10.1029/2004GC000816
- 876 Thirlwall, M.F., Upton, B.G.J. & Jenkins, C. (1994). Interaction between continental
877 lithosphere and the Iceland plume – Sr-Nd-Pb isotope geochemistry of Tertiary
878 basalts, NE Greenland. *Journal of Petrology* **35**, 839-879.
- 879 Thy, P., Lesher, C.E. & Tegner, C. (2013). Further work on experimental plagioclase
880 equilibria and the Skaergaard liquidus temperature. *American Mineralogist* **98**, 1360-
881 1367.

882 Todt, W., Cliff, R.A., Hanser, A. & Hoffmann, A.W. (1984). $^{202}\text{Pb}+^{205}\text{Pb}$ double spike
883 for lead isotopic analyses. *Terra Cognita* **4**, 209.

884 Weinstein, Y., Navon, O., Altherr, R. & Stein, M. (2006). The role of lithospheric
885 mantle heterogeneity in the generation of Plio-Pleistocene alkali basaltic suites from
886 NW Harrat Ash Shaam (Israel). *Journal of Petrology* **47**, 1017-1050.

887 Workman, R.K. & Hart, S.R., (2005) Major and trace element composition of the
888 depleted MORB mantle (DMM). *Earth and Planetary Science Letters* **231**, 53-72.

889 **FIGURE CAPTIONS**

890 Figure 1. (a) Location of the Karacadağ Volcanic Complex along with other Neogene
891 to Quaternary volcanic fields at northern margin of Arabian Plate and the locations of
892 major tectonic features in the region. The location of (b) is indicated by a black box.
893 (b) Map of the Karacadağ Volcanic Complex showing the distribution of the
894 Karacadağ and Ovabağ products and sites sampled during this work. Symbols are
895 based on geochemical discrimination (see text for details).

896 Figure 2. Plots of selected major elements versus MgO for Karacadağ and Ovabağ
897 phase lavas from Karacadağ Volcanic Complex. Fields of published data for both
898 phases are from Lustrino et al. (2012) and references therein. Data for Al Ghab and
899 Homs volcanic fields in the northern Dead Sea Fault are from Ma et al. (2011).

900 Figure 3. Plots of selected trace elements versus MgO for Karacadağ and Ovabağ
901 phase lavas from Karacadağ Volcanic Complex. Fields of published data for both
902 phases are from Lustrino et al. (2012) and references therein. Data for Al Ghab and
903 Homs volcanic fields in the northern Dead Sea Fault are from Ma et al. (2011).

904 Figure 4. Ranges of incompatible trace element concentrations in Karacadağ
905 Volcanic Complex lavas normalised to primitive mantle (McDonough and Sun, 1995).
906 Karacadağ phase (a) group K1, (b) group K2 and (c) group K3. Note the more

907 expanded scale in panel (c). Ovabağ Phase (d) group O1, (e) group O2 and (f) group
908 O3.

909 Figure 5. Plots of MgO or SiO₂ versus selected incompatible trace element ratios
910 normalised to primitive mantle (McDonough and Sun, 1995) for Karacadağ and
911 Ovabağ phase lavas from Karacadağ Volcanic Complex.

912 Figure 6. (a) ⁸⁷Sr/⁸⁶Sr versus ¹⁴³Nd/¹⁴⁴Nd, (b) ²⁰⁶Pb/²⁰⁴Pb versus ²⁰⁷Pb/²⁰⁴Pb, (c)
913 ²⁰⁶Pb/²⁰⁴Pb versus ²⁰⁸Pb/²⁰⁴Pb, and (d) Δ7/4 versus Δ8/4 for Karacadağ and Ovabağ
914 lavas from Karacadağ Volcanic Complex (KVC). Other data from KVC Siverek
915 plateau lavas (Ekici et al., 2012; Lustrino et al., 2010) and from Karasu Valley
916 (Çapan et al., 1987), NW Syria (Krienitz et al., 2006), the Dead Sea Fault in Syria
917 (DSF – Syria; Ma et al., 2011), Harrat Ash Shaam in Jordan (Shaw et al., 2003) and
918 lavas that have been attributed to a plume component beneath Afar (Deniel et al.
919 1994; Pik et al. 1999). Northern Hemisphere Reference Line in (b) and (c) from Hart
920 (1984). Black curves are models of assimilation with fractional crystallisation (De
921 Paolo, 1981) by magma with the composition of lava DK-29. Ticks marks on the
922 curves represent values for melt remaining (F) of 0.999, 0.995, 0.993, 0.99 then 0.01
923 increments to 0.95 and 0.05 increments subsequently. Note than some of these ticks
924 lie beyond the frame of each panel. UC is contamination of DK-29 by upper crust (Sr
925 = 69 ppm, Nd = 18.5 ppm, Pb = 48 ppm, ⁸⁷Sr/⁸⁶Sr = 0.764478, ¹⁴³Nd/¹⁴⁴Nd =
926 0.511398, ²⁰⁶Pb/²⁰⁴Pb = 18.598, ²⁰⁷Pb/²⁰⁴Pb = 16.026, ²⁰⁸Pb/²⁰⁴Pb = 39.746), while
927 LC is contamination by lower crust (Sr = 814 ppm, Nd = 29.94 ppm, Pb = 30 ppm,
928 ⁸⁷Sr/⁸⁶Sr = 0.709028, ¹⁴³Nd/¹⁴⁴Nd = 0.511270, ²⁰⁶Pb/²⁰⁴Pb = 16.926, ²⁰⁷Pb/²⁰⁴Pb =
929 15.622, ²⁰⁸Pb/²⁰⁴Pb = 37.804). Crustal compositions from Davidson and Wilson
930 (1989).

931 Figure 7. Plots of selected major elements versus MgO for Karacadağ phase lavas
932 from Karacadağ Volcanic Complex. Fractional crystallisation models generated using

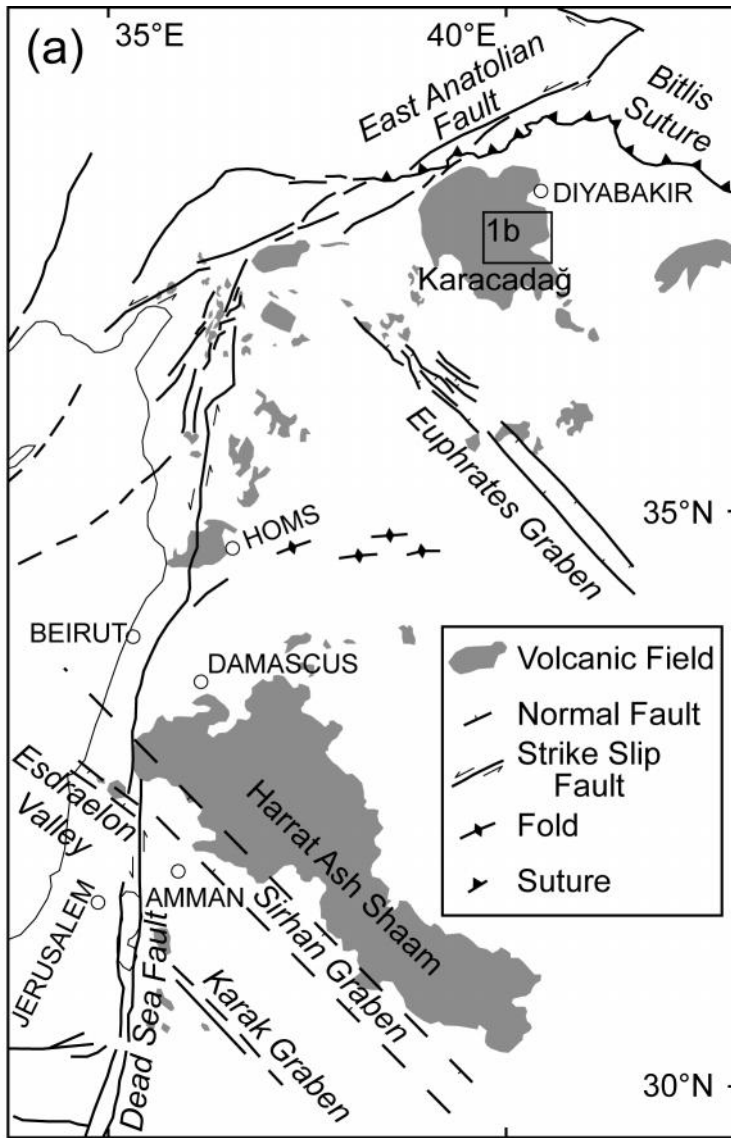
933 alphaMELTS (Smith and Asimow, 2005) for KD-102 at 5 MPa (solid line) and DK-26
934 at 22.5 MPa (dashed line). See text for more details.

935 Figure 8. (a) La/Yb versus Dy/Yb, (b) Ba/La versus La/Yb, (c) K/Nb versus K/La, and
936 (d) Sm/Zr versus La/Yb for Pliocene to Quaternary Karacadağ Volcanic Complex
937 lavas normalised to primitive mantle (McDonough and Sun, 1995). Data from Al
938 Ghab and Homs in the Dead Sea Fault (Ma et al., 2011) and Harrat Ash Shaam in
939 Jordan (Shaw et al., 2003) included for comparison. Melting models use partition
940 coefficients from Adam and Green (2011), except spinel and potassium in phases
941 not listed in that paper, which use Ma et al. (2011). Melting models for garnet- and
942 spinel-lherzolite use primitive mantle composition of McDonough and Sun (1995),
943 and modal and melting proportions of Thirlwall et al (1994). For hornblendite, the
944 initial composition and melting proportions are from Ma et al. (2011). Tick marks
945 indicate total melt fraction.

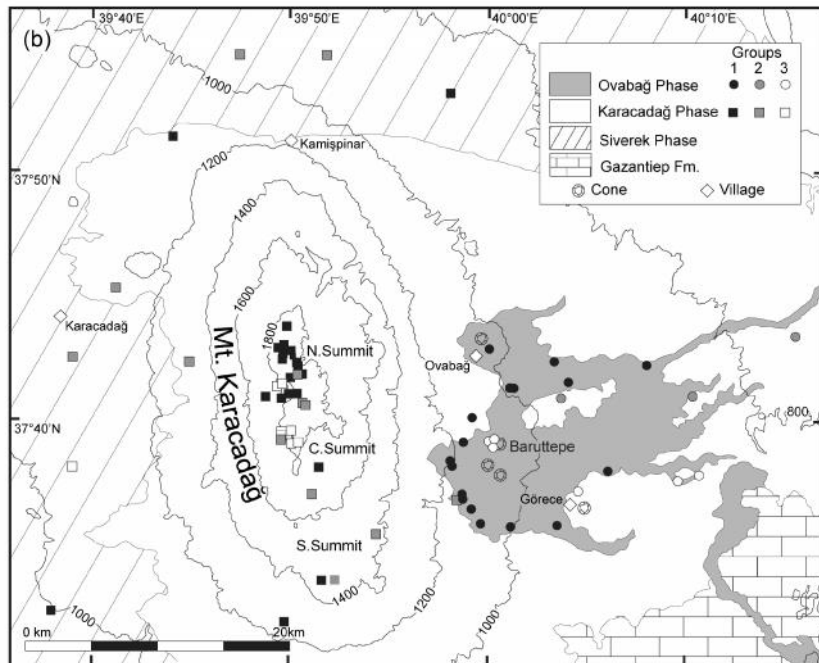
946 Figure 9. (a) K/La versus Zr/Nb, (b) La/Yb versus Rb/Ba, (c) La/Yb versus Ba/Yb,
947 and (d) K/Nb versus Ba/La for Pliocene to Quaternary Karacadağ Volcanic Complex
948 lavas normalised to primitive mantle (McDonough and Sun, 1995). For sources of
949 comparator data see caption to Fig. 6. Melting models use abundances of primitive
950 mantle. Garnet-lherzolite (Gt-LH) and spinel-lherzolite (Sp-LH) models are as
951 described in caption to Figure 6, except that large ion lithophile elements were
952 increased by a factor of two (Sisson et al., 2009). Modal and melting proportions are
953 from Ma et al (2011) for amphibole-garnet lherzolite (AG-LH) and from Sisson et al.
954 (2009) for phlogopite-garnet lherzolite (PG-LH). Tick marks indicate total melt
955 fractions.

956 Figure 10. Sketch of petrogenesis at Mt Karacadağ. Siverek plateau basalts were
957 erupted during the Miocene and are the substrate onto which the Karacadağ volcano
958 was erupted. The scale of the vertical axis is schematic and is not intended to be
959 regarded as linear. Constraints on the depth of the upper – lower crust boundary

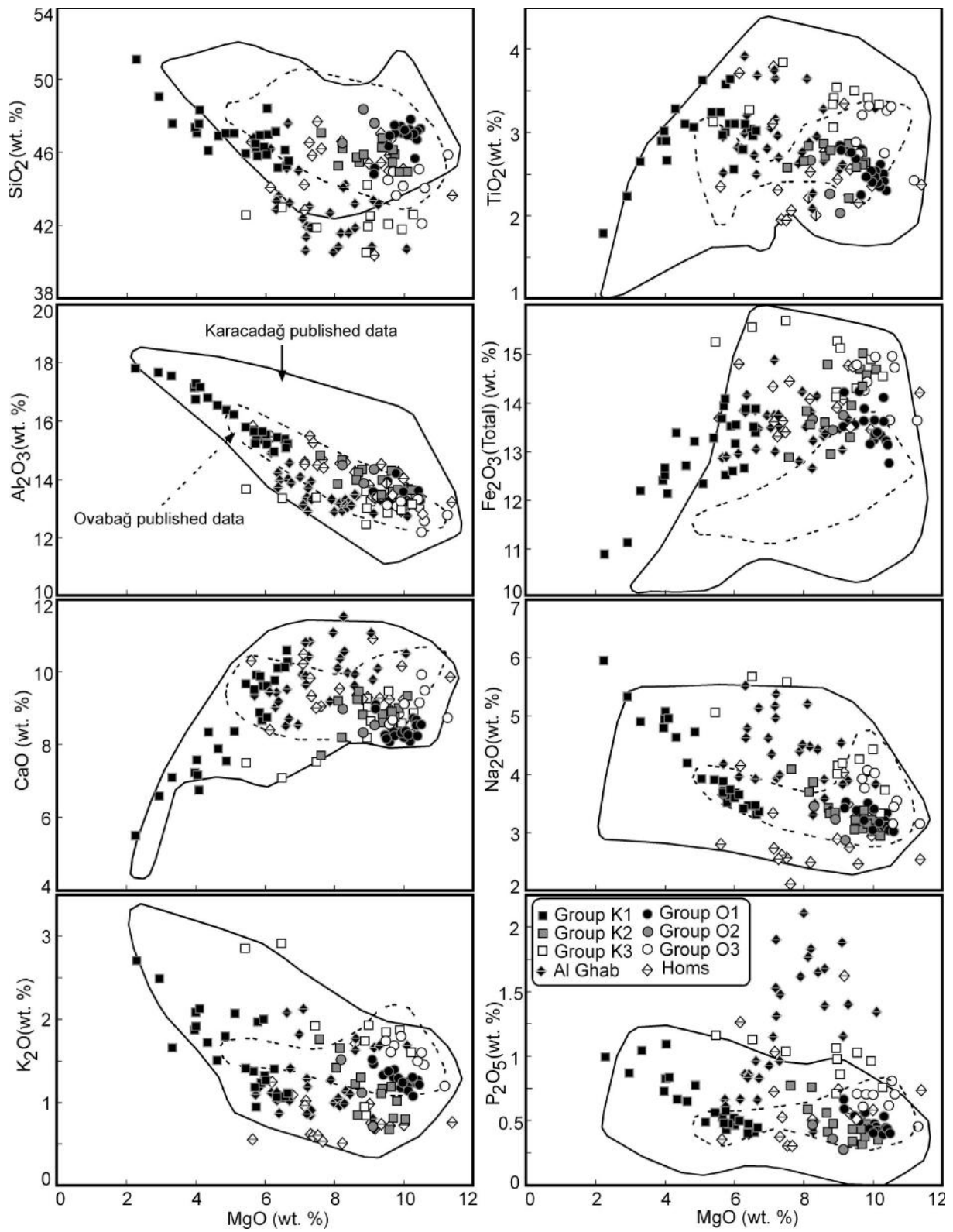
960 come from geophysics and xenolith petrology (see text for details). Differentiation
961 depths are from alphaMELTS models. Group K1 and K2 lavas share similar sources
962 that represent polybaric melting but with a relatively large contribution from the spinel
963 stability field, while group K3 lavas contain a larger contribution from deeper, garnet-
964 bearing mantle. Group K2 lavas have experienced relatively restricted amounts of
965 differentiation close to the upper – lower crust boundary and are found along the
966 length of the volcano. Lavas of group K1 occur predominantly in the north and
967 developed when group K2 magma experienced more extensive differentiation at the
968 upper – lower crustal transition. Group K3 lavas experienced small amounts of
969 differentiation close to the base of the lithosphere.



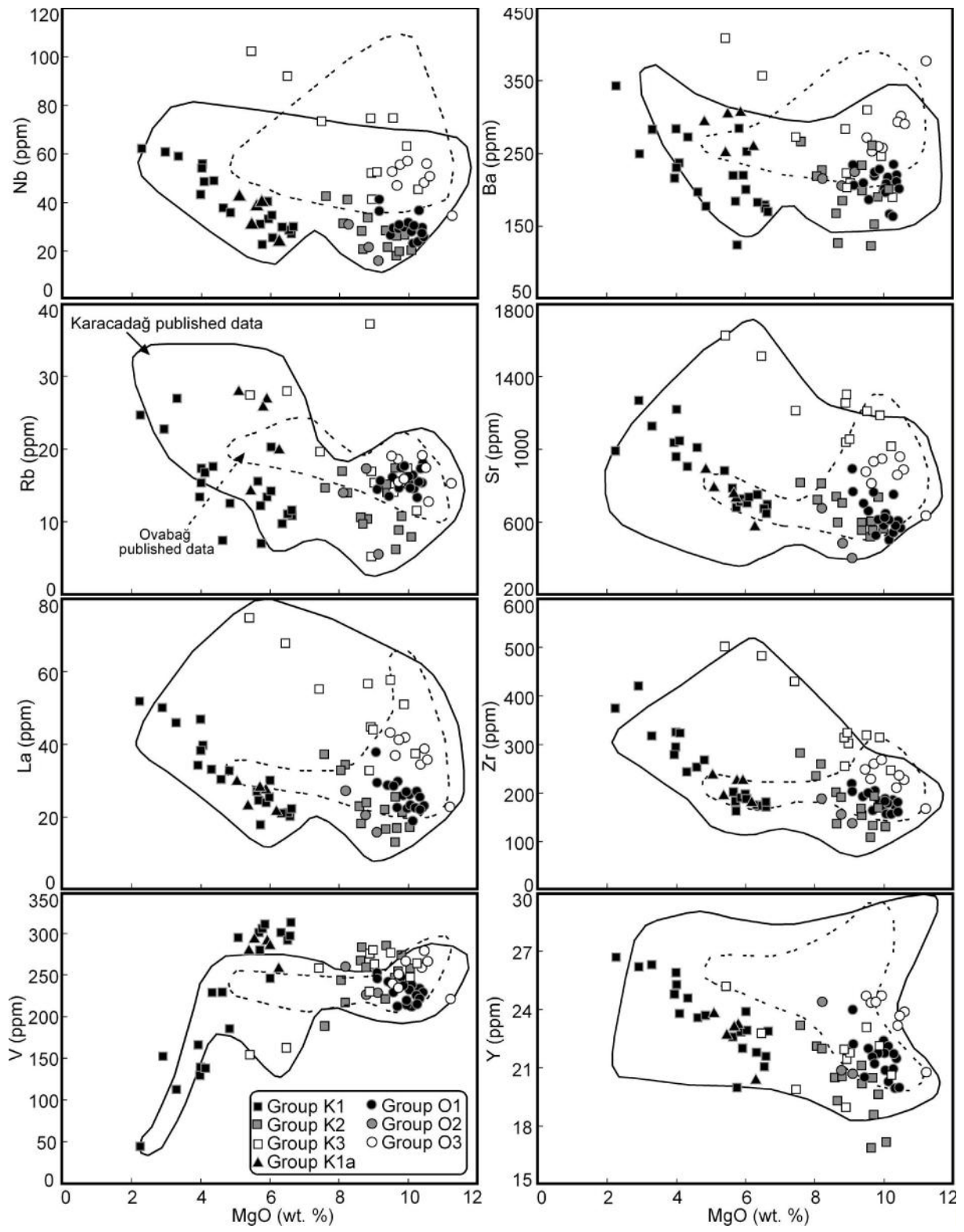
Karacada 1a



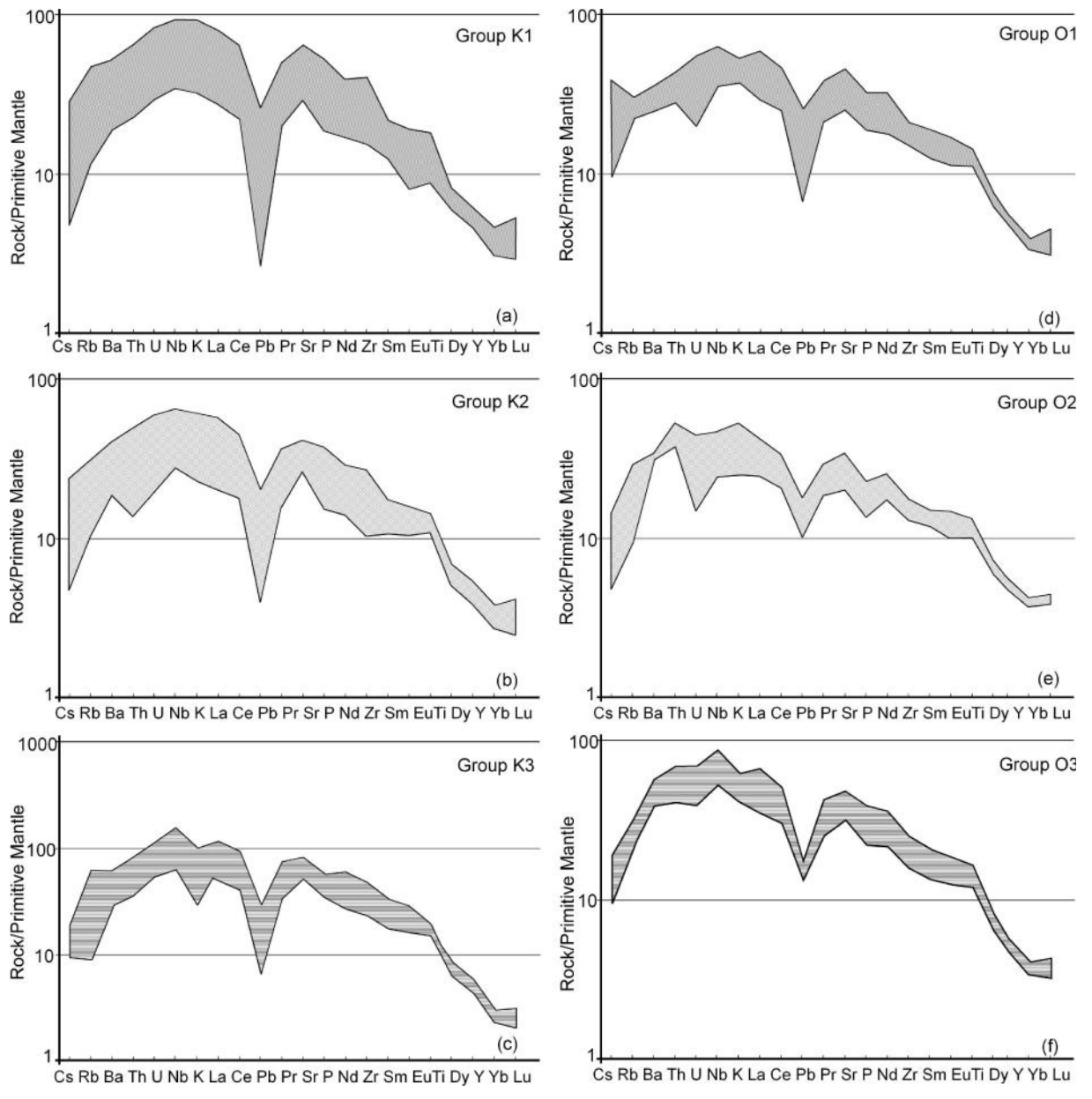
Karacada 1b



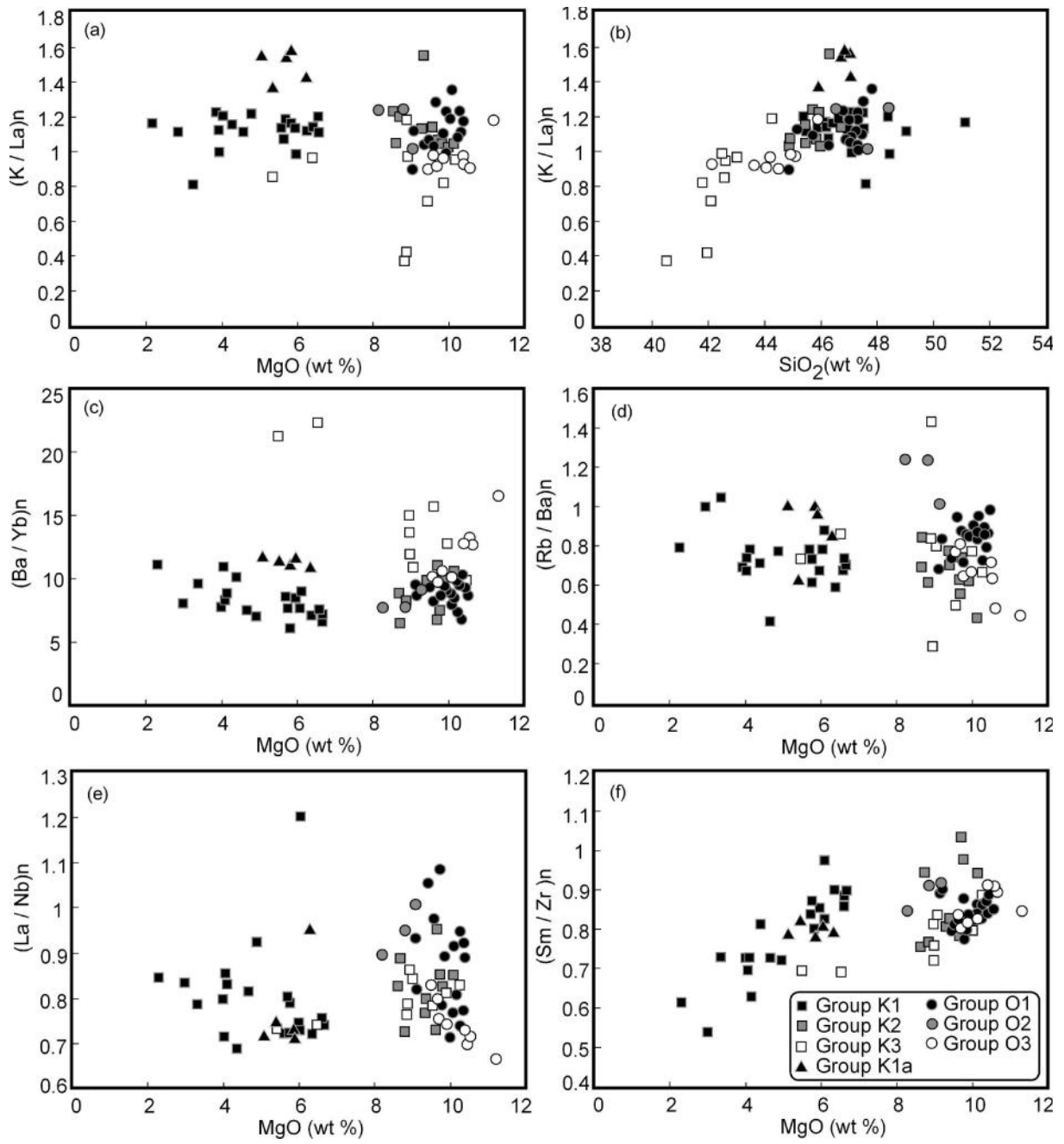
Karacada 2



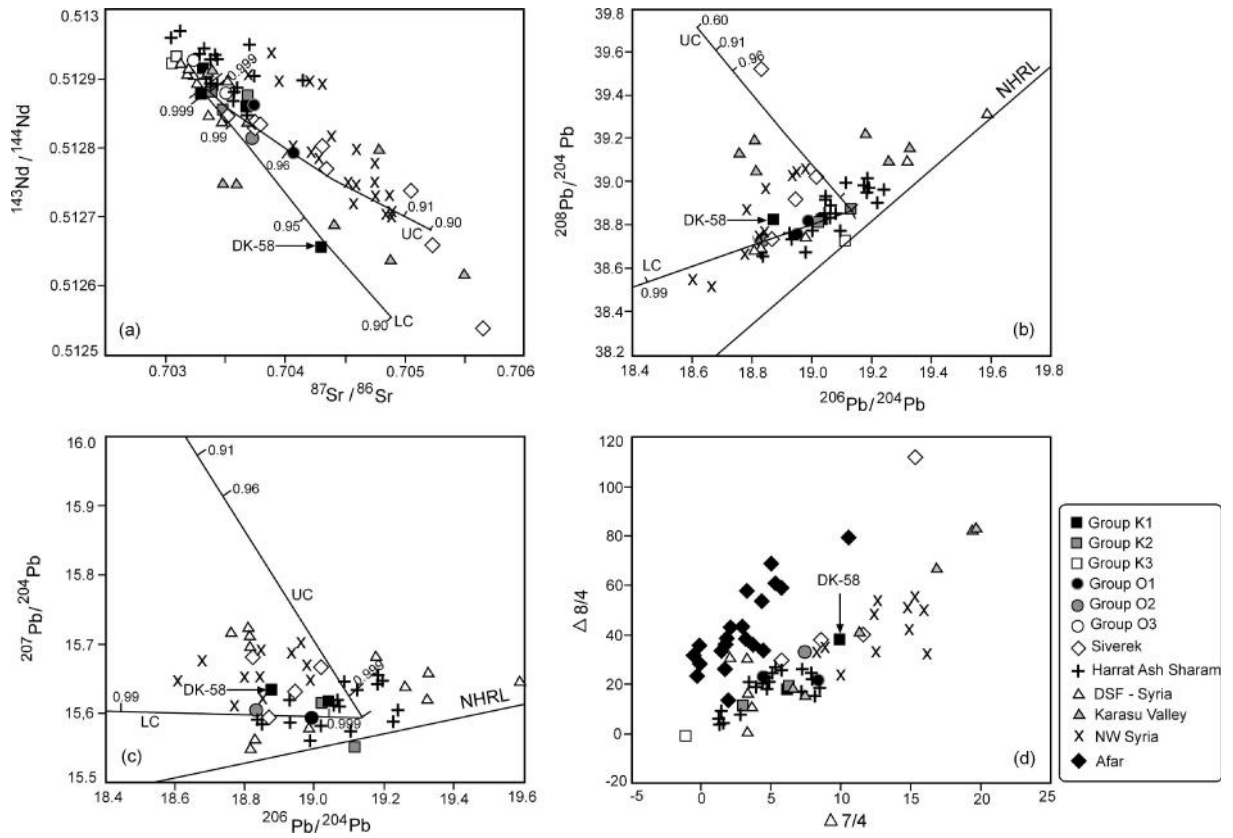
Karacada 3



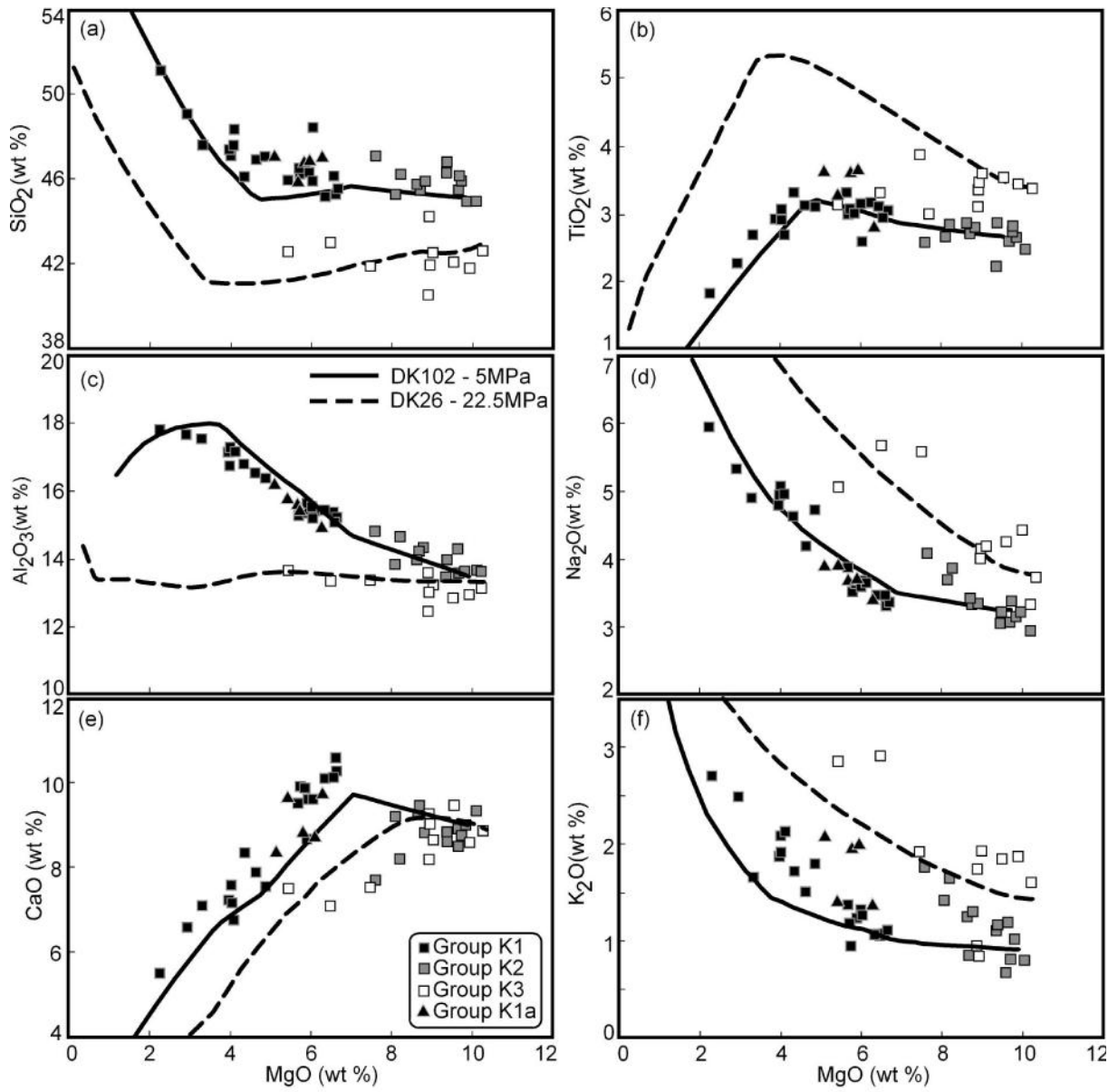
Karacada 4



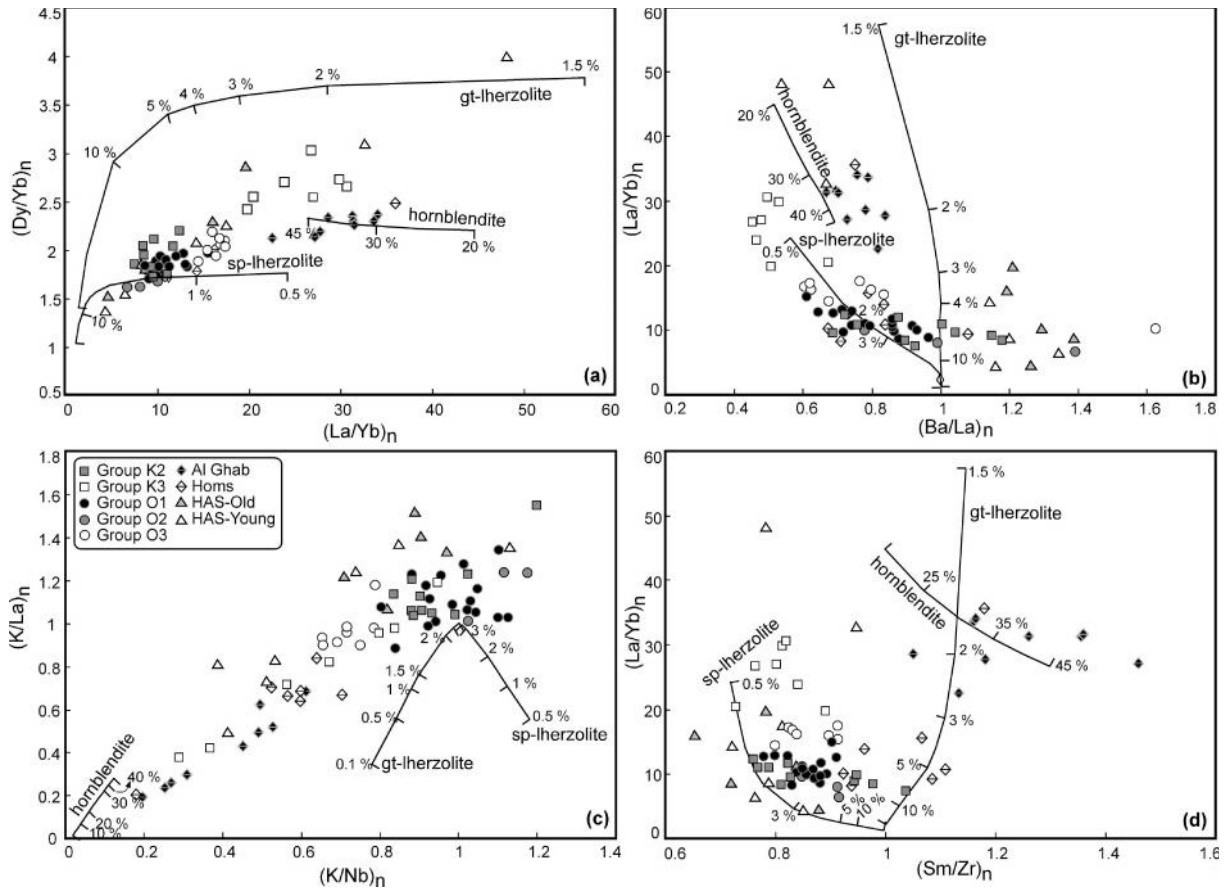
Karacada 5



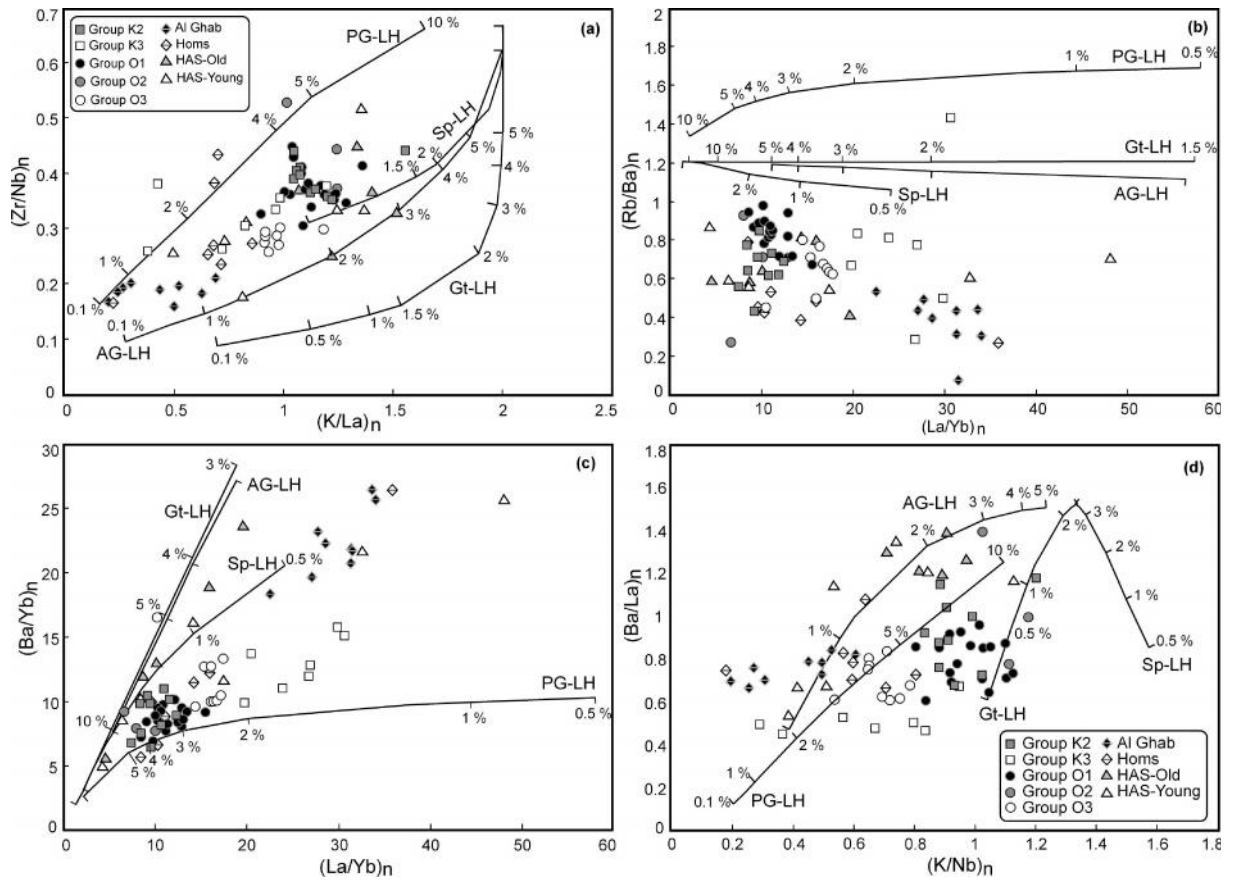
Karacada 6



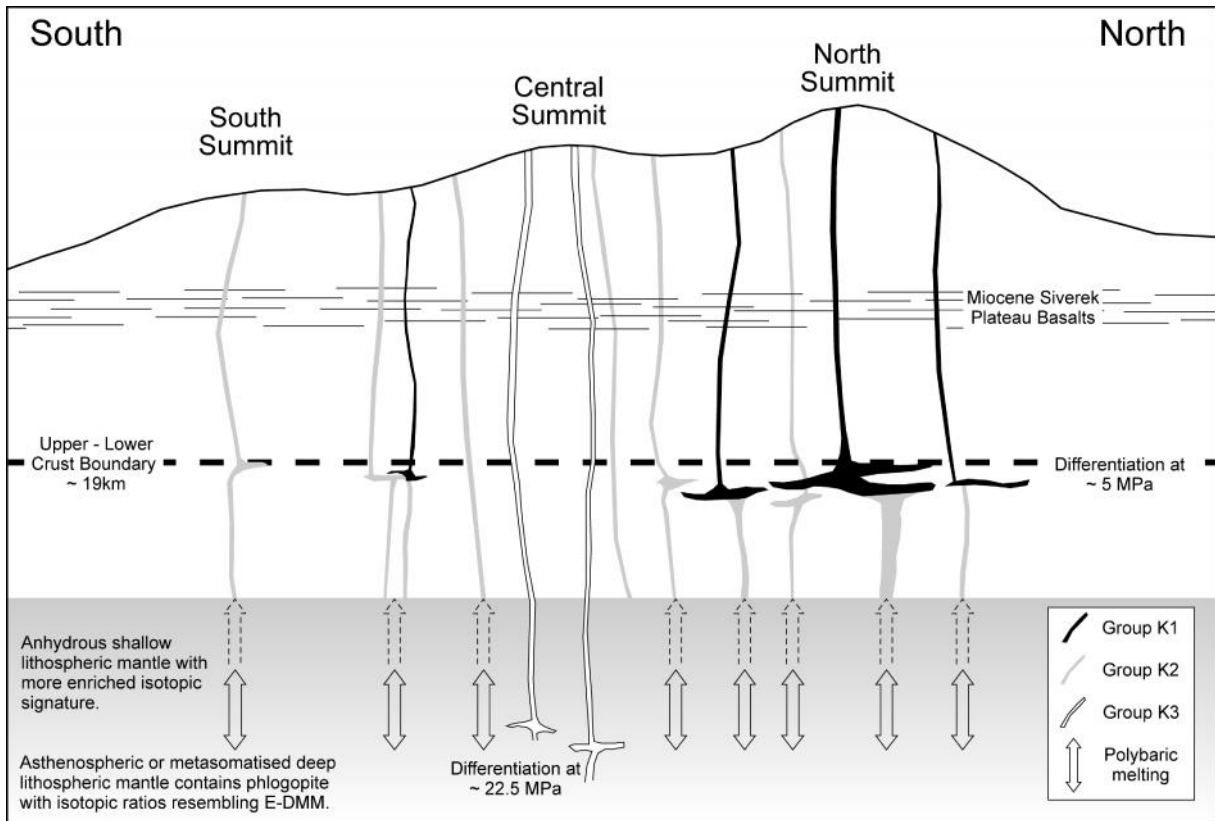
Karacada 7



Karacada 8



Karacada 9



1 Table 1: Major and trace element compositions of Karacadağ and Ovabağ lavas.

Sample	DK-1 (K1)	DK-2 (K1)	DK-3 (K1)	DK-4 (K1)	DK-5 (K1)	DK-6 (K1)	DK-7 (K1)	DK-8 (K1)
Latitude	37°42'35.64"N	37°42'22.44"N	37°42'55.98"N	37°42'47.34"N	37°42'49.38"N	37°42'43.32"N	37°42'15.72"N	37°42'5.22"N
Longitude	39°49'43.20"E	39°49'42.18"E	39°49'45.60"	39°49'37.26"E	39°49'28.68"E	39°50'6.30"E	39°50'23.52"E	39°50'27.12"E
SiO ₂	46.15	46.12	45.92	45.91	46.33	45.48	46.93	48.34
TiO ₂	3.04	3.29	3.10	3.25	3.10	3.03	3.10	2.67
Al ₂ O ₃	15.38	16.82	15.44	15.60	15.40	15.19	16.55	17.22
Fe ₂ O ₃	13.49	13.38	13.53	13.67	13.51	13.86	12.70	12.11
MgO	6.55	4.33	6.02	5.65	5.92	6.63	4.62	4.08
MnO	0.17	0.18	0.17	0.17	0.17	0.17	0.17	0.17
CaO	10.10	8.33	9.61	9.52	9.61	10.25	7.87	6.75
Na ₂ O	3.46	4.64	3.67	3.88	3.70	3.39	4.20	4.96
K ₂ O	1.06	1.71	1.29	1.37	1.24	1.09	1.51	2.13
P ₂ O ₅	0.42	0.66	0.49	0.52	0.46	0.44	0.65	0.83
Cr ₂ O ₃	0.019	0.001	0.001	0.007	0.013	0.020	0.014	0.007
LOI	-0.2	0.2	0.4	0.1	0.1	0.1	1.4	0.4
Total	99.65	99.66	99.66	99.66	99.66	99.67	99.71	99.67
Ni	72	20	55	54	67	69	31	28
Sc	24	13	21	20	22	24	14	11
V	293	229	290	297	292	313	229	139
Co	79.7	59.4	70.9	63.3	63.3	64.5	74.5	46.1
Cu	64.5	27.2	63.2	55.5	63.3	65.6	25.1	31.0
Zn	82	77	81	93	63	84	43	83
Ga	23.2	26.3	23.8	24.9	24.9	24.7	24.4	24.9
Rb	11.1	17.7	14.3	15.6	13.5	11.0	7.5	16.8
Sr	678	909	734	784	715	697	1009	1048
Y	21.1	24.6	22.9	22.6	22.0	22.9	23.6	23.8
Zr	173	243	198	202	189	177	253	323
Nb	28.4	48.9	34.5	37.7	33.3	29.9	37.8	48.5
Cs	0.3	0.4	0.3	0.4	0.4	0.2	0.3	0.2
Ba	179	273	201	220	220	170	197	237
La	21.1	33.2	25.4	27.0	24.1	22.0	30.4	39.7
Ce	47.7	71.1	55.7	58.3	53.2	49.0	67.6	85.0
Pr	6.11	8.86	7.08	7.36	6.70	6.33	8.53	10.33
Nd	26.1	36.6	29.3	31.3	28.5	26.6	34.7	41.0
Sm	5.76	7.66	6.32	6.56	6.24	6.14	7.13	7.86
Eu	2.14	2.67	2.28	2.33	2.22	2.24	2.65	2.85
Gd	5.95	7.19	6.54	6.56	6.09	6.32	6.87	7.31
Tb	0.92	1.07	0.95	0.99	0.95	0.96	1.01	1.04
Dy	4.49	5.29	4.80	4.75	4.66	4.69	5.03	5.15
Ho	0.84	0.94	0.88	0.88	0.82	0.88	0.91	0.89
Er	2.00	2.35	2.17	2.13	2.10	2.14	2.22	2.25
Tm	0.31	0.33	0.33	0.31	0.30	0.30	0.31	0.34
Yb	1.60	1.79	1.74	1.71	1.73	1.71	1.74	1.79
Lu	0.26	0.27	0.26	0.25	0.25	0.25	0.25	0.27
Hf	4.4	5.6	4.9	4.9	4.7	4.7	5.5	7.4
Ta	1.6	2.7	2.0	2.2	2.0	1.7	2.2	2.8
Pb	2.0	1.0	1.9	1.1	1.9	1.2	0.4	0.7
Th	2.1	3.1	2.5	2.7	2.5	2.1	2.9	3.4
U	0.7	1.1	0.9	0.9	0.7	0.7	1.0	1.3

2

3

4

Sample	DK-9 (K1)	DK-10 (K1)	DK-11 (K2)	DK-13 (K3)	DK-14 (K3)	DK-15 (K1a)	DK-16 (K1a)	DK-17 (K1a)
Latitude	37°41'48.60"N	37°41'46.80"N	37°41'46.08"N	37°41'24.90"N	37°41'19.02"N	37°40'54.30"N	37°40'51.24"N	37°41'1.74"N
Longitude	39°50'40.56"E	39°50'34.80"E	39°50'26.16"E	39°49'40.86"E	39°49'24.66"E	39°48'51.06"E	39°49'39.24"E	39°50'1.02"E
SiO ₂	47.40	49.04	45.86	40.53	42.09	46.76	47.05	46.85
TiO ₂	2.90	2.24	2.79	3.35	3.51	3.58	3.60	3.59
Al ₂ O ₃	17.17	17.70	14.33	12.49	12.89	15.56	16.23	15.65
Fe ₂ O ₃	12.41	11.12	12.93	14.16	14.31	12.54	12.33	12.66
MgO	3.95	2.92	8.81	8.90	9.53	5.81	5.10	5.88
MnO	0.17	0.18	0.16	0.18	0.18	0.15	0.15	0.15
CaO	7.20	6.57	8.79	9.28	9.46	8.83	8.36	8.65
Na ₂ O	4.80	5.33	3.33	4.02	4.26	3.64	3.90	3.59
K ₂ O	1.87	2.49	1.30	0.95	1.85	1.96	2.07	1.99
P ₂ O ₅	0.72	0.87	0.47	1.06	1.03	0.50	0.52	0.51
Cr ₂ O ₃	0.004	0.002	0.046	0.036	0.034	0.018	0.012	0.017
LOI	1.1	1.2	0.8	4.7	0.3	0.3	0.3	0.1
Total	99.68	99.63	99.63	99.63	99.49	99.65	99.65	99.65
Ni	20	20	132	184	181	70	51	61
Sc	7	7	21	17	18	19	17	19
V	166	152	260	278	277	305	295	310
Co	53.1	42.1	74.0	71.1	78.0	58.8	60.3	60.3
Cu	26.7	22.6	41.0	32.2	61.9	46.7	43.5	46.0
Zn	59	88	76	48	107	84	87	86
Ga	23.8	23.8	22.4	26.1	26.6	25.4	25.7	25.7
Rb	13.5	22.8	10.4	37.2	14.2	25.8	27.8	26.7
Sr	1038	1267	707	1262	1210	742	793	729
Y	24.8	26.2	20.6	22.0	23.1	23.1	23.8	22.9
Zr	278	421	193	314	319	224	235	224
Nb	43.4	60.9	33.6	74.8	74.8	39.6	42.4	40.2
Cs	0.2	0.2	0.2	0.2	0.3	0.5	0.6	0.6
Ba	216	250	186	285	311	285	306	306
La	34.2	50.1	24.1	56.6	57.8	28.4	30.0	28.4
Ce	65.6	102.8	52.1	111.7	115.9	61.5	64.5	62.5
Pr	9.37	12.19	6.42	13.42	13.70	7.86	8.08	7.72
Nd	38.5	47.6	26.2	54.1	53.3	32.4	34.0	32.8
Sm	7.83	8.82	5.71	9.93	10.01	6.82	7.15	7.02
Eu	2.79	2.92	2.06	3.33	3.46	2.32	2.38	2.34
Gd	7.29	7.69	5.63	8.86	8.99	6.53	6.78	6.65
Tb	1.09	1.10	0.86	1.15	1.24	0.99	1.02	1.02
Dy	5.53	5.31	4.25	5.13	5.51	4.76	4.95	5.04
Ho	0.91	0.99	0.76	0.83	0.86	0.85	0.86	0.88
Er	2.33	2.36	1.90	1.77	1.84	2.12	2.19	2.21
Tm	0.31	0.36	0.26	0.24	0.25	0.31	0.31	0.30
Yb	1.84	2.05	1.53	1.26	1.32	1.70	1.74	1.77
Lu	0.28	0.31	0.22	0.18	0.19	0.26	0.26	0.26
Hf	6.4	9.3	4.6	7.0	7.1	5.6	5.7	5.6
Ta	2.6	3.6	2.0	3.8	3.9	2.3	2.4	2.4
Pb	1.0	3.1	0.9	1.5	3.3	2.8	2.9	2.8
Th	2.5	5.1	2.2	5.5	5.2	3.5	4.1	3.7
U	1.1	1.4	0.7	2.0	1.9	1.1	1.2	1.1

5

6

7

Sample	DK-18 (K1)	DK-19 (K1)	DK-20 (K1)	DK-21 (K1)	DK-22 (K-3)	DK-23 (K-2)	DK-24 (K-3)	DK-25 (K-3)
Latitude	37°41'10.93"N	37°41'18.74"N	37°41'9.11"N	37°41'2.22"N	37°39'5.76"N	37°39'13.44"N	37°39'23.94"N	37°39'30.42"N
Longitude	39°49'47.22"E	39°49'57.09"E	39°50'16.70"E	39°50'25.62"E	39°50'12.30"E	39°49'39.48"E	39°49'39.84"E	39°49'40.56"E
SiO ₂	47.61	51.11	47.03	47.46	41.80	45.44	41.90	42.60
TiO ₂	2.65	1.79	3.07	3.02	3.43	2.61	3.85	3.13
Al ₂ O ₃	17.56	17.82	16.40	17.29	13.01	14.27	13.42	13.71
Fe ₂ O ₃	12.19	10.88	13.18	12.65	14.93	14.68	15.70	15.27
MgO	3.30	2.25	4.85	4.00	9.92	9.65	7.46	5.43
MnO	0.18	0.19	0.18	0.18	0.18	0.17	0.17	0.20
CaO	7.09	5.52	7.55	7.16	8.60	8.91	7.54	7.51
Na ₂ O	4.91	5.95	4.73	5.07	4.43	3.08	5.60	5.07
K ₂ O	1.66	2.70	1.80	1.92	1.87	0.67	1.92	2.86
P ₂ O ₅	1.04	0.99	0.77	0.82	0.96	0.32	1.03	1.17
Cr ₂ O ₃	0.002	0.002	0.010	0.002	0.027	0.038	0.015	0.010
LOI	1.5	0.5	0.1	0.1	0.3	-0.2	0.9	2.5
Total	99.68	99.69	99.68	99.67	99.49	99.66	99.51	99.45
Ni	20	20	41	20	206	223	119	76
Sc	9	9	14	10	17	21	10	8
V	112	44	185	129	247	246	258	155
Co	83.7	47.9	52.1	42.9	76.7	79.5	88.4	102.4
Cu	20.9	15.3	41.3	24.3	43.5	81.3	35.3	29.4
Zn	101	99	103	97	74	93	68	127
Ga	25.6	26.6	23.6	25.0	26.5	20.5	30.3	32.0
Rb	27.0	24.7	12.5	15.5	17.5	6.3	19.7	27.5
Sr	1132	991	896	960	1192	530	1214	1628
Y	26.3	26.7	23.7	25.9	22.1	16.9	19.9	25.2
Zr	318	375	267	294	315	109	430	501
Nb	59.2	62.2	36.3	54.2	63.6	18.3	73.6	102.5
Cs	0.4	0.3	0.2	0.2	0.2	0.1	0.3	0.4
Ba	283	343	178	231	248	124	274	409
La	46.0	51.9	33.1	38.3	51.0	13.2	55.2	74.8
Ce	97.0	107.3	72.9	83.2	104.4	30.2	115.7	155.8
Pr	12.10	12.84	9.14	10.45	12.75	4.00	13.89	18.88
Nd	47.3	49.8	37.2	42.0	51.8	17.7	55.8	74.0
Sm	8.99	8.93	7.47	8.28	9.76	4.37	10.65	13.50
Eu	1.24	2.97	2.54	2.86	3.32	1.62	3.46	4.38
Gd	8.04	7.77	6.67	7.54	8.58	4.46	9.03	11.26
Tb	1.17	1.12	0.98	1.12	1.17	0.70	1.13	1.44
Dy	5.52	5.29	4.82	5.33	5.03	3.44	4.86	5.80
Ho	0.97	0.98	0.87	0.98	0.82	0.64	0.75	0.95
Er	2.36	2.30	2.09	2.38	1.70	1.48	1.44	1.88
Tm	0.36	0.35	0.30	0.33	0.24	0.22	0.19	0.24
Yb	1.96	2.05	1.68	1.88	1.29	1.21	1.02	1.28
Lu	0.29	0.30	0.25	0.28	0.17	0.17	0.14	0.17
Hf	6.8	8.0	5.8	6.7	7.1	2.7	9.7	11.1
Ta	3.2	3.6	2.1	3.0	3.4	1.0	4.3	5.5
Pb	0.4	1.9	0.6	1.0	1.7	0.8	1.5	4.4
Th	3.5	4.5	2.2	3.1	4.7	1.1	5.1	6.6
U	1.3	1.7	1.0	1.2	1.8	0.4	2.1	2.3

8

9

10

Sample	DK-26 (K-3)	DK-27 (K-3)	DK-28 (K-3)	DK-29 (K-2)	DK-30 (K-2)	DK-31 (K1)	DK-32 (K1)	DK-52 (K-2)
Latitude	37°39'28.98"N	37°39'26.10"N	37°39'22.62"N	37°40'35.82"N	37°40'40.32"N	37°42'29.70"N	37°43'40.38"N	37°42'31.26"N
Longitude	39°50'9.78"E	39°50'6.66"E	39°50'3.00"E	39°50'52.02"E	39°50'42.84"E	39°50'11.28"E	39°49'51.96"E	39°38'59.04"E
SiO ₂	42.60	43.02	42.54	47.07	46.26	45.37	45.20	44.90
TiO ₂	3.35	3.28	3.55	2.58	2.84	2.97	3.10	2.48
Al ₂ O ₃	13.30	13.39	13.30	14.83	14.65	15.11	15.44	13.64
Fe ₂ O ₃	14.56	15.57	15.15	12.86	13.54	13.40	13.88	14.67
MgO	10.25	6.48	9.02	7.60	8.21	6.60	6.35	10.09
MnO	0.17	0.19	0.18	0.18	0.18	0.17	0.17	0.17
CaO	8.85	7.10	8.65	7.70	8.20	10.58	10.09	9.32
Na ₂ O	3.73	5.69	4.20	4.09	3.86	3.33	3.46	2.97
K ₂ O	1.60	2.92	1.93	1.76	1.65	1.09	1.06	0.80
P ₂ O ₅	0.76	1.14	0.86	0.77	0.76	0.43	0.45	0.35
Cr ₂ O ₃	0.037	0.010	0.027	0.036	0.041	0.021	0.012	0.040
LOI	0.3	0.7	0.1	0.1	0.1	0.6	0.0	0.2
Total	99.54	99.49	99.53	99.60	100.2	99.67	99.24	99.65
Ni	225	99	175	129	151	71	67	223
Sc	19	7	18	16	18	25	183	202
V	265	163	263	189	217	297	301	258
Co	87.7	60.2	77.6	62.2	67.8	65.4	71.4	80.1
Cu	62.1	25.0	57.1	47.9	56.5	62.3	63.1	67.8
Zn	103	100	119	85	92	83	93	92
Ga	24.8	31.0	27.0	24.1	23.2	23.0	24.1	20.3
Rb	11.7	28.1	15.5	14.7	14.0	11.5	9.8	8.0
Sr	1020	1511	1059	816	810	652	750	579
Y	20.7	22.8	21.8	23.2	22.0	21.6	21.8	17.2
Zr	248	482	303	282	260	173	176	130
Nb	45.8	92.3	52.6	42.6	41.1	27.8	29.7	20.6
Cs	0.2	0.4	0.2	0.1	0.2	0.2	0.1	0.1
Ba	192	358	209	266	228	173	183	202
La	37.4	67.8	44.1	37.2	34.2	20.4	21.2	17.3
Ce	81.0	141.4	95.5	75.0	72.3	46.1	48.3	38.6
Pr	10.00	17.39	11.91	9.34	8.80	6.01	6.44	4.96
Nd	40.7	68.9	48.8	36.2	36.0	25.3	26.7	20.9
Sm	8.53	12.90	9.84	7.11	7.09	5.95	6.14	4.74
Eu	2.78	4.13	3.27	2.43	2.33	1.99	2.26	1.71
Gd	7.53	10.76	8.44	6.52	6.30	5.67	6.14	4.76
Tb	1.04	1.35	1.15	0.93	0.94	0.91	1.05	0.75
Dy	4.78	5.76	5.21	4.39	4.18	4.37	4.83	3.61
Ho	0.79	0.86	0.82	0.82	0.83	0.80	0.99	0.68
Er	1.76	1.64	1.79	2.09	1.92	2.00	2.20	1.69
Tm	0.25	0.20	0.23	0.29	0.27	0.28	0.41	0.24
Yb	1.29	1.07	1.26	1.69	1.64	1.59	1.72	1.29
Lu	0.18	0.14	0.21	0.24	0.25	0.24	0.36	0.23
Hf	5.7	10.9	7.0	6.6	5.9	4.3	4.4	3.7
Ta	2.6	5.0	3.0	2.4	2.3	1.5	1.7	1.2
Pb	2.3	1.3	2.5	2.0	1.5	1.6	1.8	1.5
Th	2.9	5.7	3.3	3.4	2.7	2.2	2.1	1.9
U	1.1	2.3	1.4	1.2	1.1	0.7	0.6	0.6

11

12

13

Sample	DK-53 (K-2)	DK-55 (K-1)	DK-56 (K-2)	DK-57 (K-2)	DK-58 (K-1a)	DK-81 (K-3)	DK-83 (K-1)	DK-84 (K-2)
Latitude	37°45'14.46"N	37°51'24.90"N	37°54'40.50"N	37°54'40.20"N	37°53'10.32"N	37°39'5.46"N	37°38'10.08"N	37°37'6.72"N
Longitude	39°41'6.72"E	39°43'59.04"E	39°47'18.36"E	39°51'42.12"E	39°57'57.24"E	39°50'29.58"E	39°51'30.06"E	39°51'10.68"E
SiO ₂	45.85	48.42	46.07	45.25	47.03	44.25	47.12	46.29
TiO ₂	2.77	2.56	2.63	2.66	2.80	3.07	2.90	2.87
Al ₂ O ₃	13.50	15.23	13.53	13.85	14.94	13.64	16.75	13.96
Fe ₂ O ₃	14.99	13.17	14.33	13.81	12.60	14.22	12.50	13.93
MgO	9.73	6.03	9.67	8.09	6.28	8.92	4.00	9.39
MnO	0.17	0.16	0.16	0.17	0.15	0.17	0.18	0.17
CaO	8.78	8.70	8.48	9.19	9.71	8.20	7.58	8.62
Na ₂ O	3.11	3.64	3.38	3.70	3.44	4.17	4.95	3.06
K ₂ O	0.80	1.32	1.19	1.42	1.37	1.74	2.09	1.15
P ₂ O ₅	0.38	0.52	0.43	0.59	0.39	0.71	1.09	0.34
Cr ₂ O ₃	0.037	0.023	0.041	0.034	0.030	0.035	0.002	0.030
LOI	-0.5	-0.1	-0.3	0.9	1.0	0.4	0.5	-0.2
Total	99.65	99.68	99.65	99.67	99.72	99.56	99.63	99.64
Ni	224	51	208	182	106	193	20	207
Sc	153	253	261	219	260	224	284	20
V	254	246	244	244	258	231	139	285
Co	80.6	54.6	73.4	69.9	58.7	71.4	47.8	81.2
Cu	74.1	39.3	57.4	58.1	50.6	51.4	23.0	51.8
Zn	91	102	92	93	72	106	93	90
Ga	21.5	23.3	22.4	23.0	21.0	24.3	25.9	22.8
Rb	8.9	20.3	17.4	17.0	20.1	17.0	17.4	14.1
Sr	546	714	604	722	580	1039	1224	555
Y	18.6	23.9	20.5	22.1	20.4	19.0	25.3	20.2
Zr	133	188	196	235	177	256	324	157
Nb	20.1	25.4	27.4	31.4	22.9	41.9	55.6	21.9
Cs	0.3	0.3	0.5	0.4	0.5	0.2	0.2	0.2
Ba	153	253	261	219	260	224	284	199
La	16.9	30.1	25.7	32.7	21.5	32.7	46.9	16.6
Ce	39.1	64.7	54.4	70.4	47.0	68.5	95.8	36.2
Pr	5.05	8.25	6.76	8.87	6.00	8.60	11.89	5.02
Nd	21.4	33.5	29.0	36.1	25.5	34.0	48.2	21.3
Sm	5.02	7.09	5.97	6.90	5.43	7.20	8.73	4.92
Eu	1.87	2.31	2.01	2.33	1.85	2.50	2.98	1.77
Gd	5.25	6.89	5.78	6.70	5.43	6.28	7.45	4.75
Tb	0.78	0.99	0.85	0.95	0.81	0.91	1.09	0.75
Dy	4.06	4.91	4.28	4.67	4.23	4.26	5.35	4.23
Ho	0.72	0.89	0.78	0.83	0.73	0.65	0.90	0.71
Er	1.75	2.22	1.90	1.92	1.82	1.62	2.28	1.77
Tm	0.26	0.31	0.29	0.26	0.28	0.20	0.31	0.25
Yb	1.36	1.89	1.59	1.63	1.59	1.09	1.73	1.35
Lu	0.24	0.32	0.26	0.28	0.27	0.15	0.24	0.20
Hf	3.6	5.0	4.8	5.6	4.6	6.1	6.8	4.1
Ta	1.2	1.5	1.6	1.9	1.4	2.6	3.4	1.4
Pb	1.9	3.9	3.0	3.0	2.7	1.0	1.8	1.2
Th	2.2	3.6	3.0	3.8	2.5	2.9	4.1	1.9
U	0.5	8.0	1.0	1.2	0.8	1.1	1.5	0.7

14

15

16

Sample	DK-90 (K-2)	DK-93 (K-1)	DK-95 (K-2)	DK-97 (K-1)	DK-98 (K-1a)	DK-99 (K-3)	DK-102 (K-2)	DK-106 (K-2)
Latitude	37°35'32.28"N	37°33'45.60"N	37°33'44.16"N	37°32'4.80"N	37°32'25.92"N	37°38'13.32"N	37°42'24.60"N	37°36'53.76"N
Longitude	39°54'22.38"E	39°51'39.24"E	39°52'19.38"E	39°49'47.34"E	39°38'4.86"E	39°39'9.06"E	39°44'58.02"E	39°58'29.16"E
SiO ₂	46.81	46.24	45.48	46.55	45.93	41.96	44.91	45.72
TiO ₂	2.21	2.99	2.72	3.00	3.22	3.42	2.65	2.87
Al ₂ O ₃	13.50	15.30	14.18	15.45	15.77	13.08	13.52	14.01
Fe ₂ O ₃	13.27	13.93	14.79	14.08	13.27	15.29	14.55	13.57
MgO	9.37	5.71	8.68	5.75	5.42	8.94	9.84	8.64
MnO	0.17	0.17	0.18	0.17	0.16	0.18	0.19	0.17
CaO	8.82	9.92	9.45	9.88	9.64	9.03	9.00	9.25
Na ₂ O	3.24	3.70	3.34	3.53	3.88	4.17	3.19	3.42
K ₂ O	1.11	1.18	0.85	0.94	1.40	0.84	1.02	1.25
P ₂ O ₅	0.43	0.57	0.41	0.43	0.56	0.98	0.46	0.56
Cr ₂ O ₃	0.043	0.018	0.039	0.011	0.011	0.030	0.041	0.047
LOI	0.7	-0.1	0.5	-0.1	0.4	1.6	0.2	0.1
Total	99.64	99.67	99.66	99.70	99.66	99.53	99.61	99.64
Ni	205	78	165	51	53	191	227	145
Sc	19	21	21	21	18	16	20	19
V	222	281	284	302	280	279	273	267
Co	69.7	62.1	71.7	63.0	55.5	69.3	79.9	64.3
Cu	38.2	56.7	74.2	49.7	64.5	44.8	59.7	42.6
Zn	92	81	94	79	71	99	77	82
Ga	21.4	24.0	21.3	22.5	23.9	25.9	21.1	21.3
Rb	15.1	12.3	9.8	7.0	14.4	5.4	10.8	10.6
Sr	597	758	599	683	883	1302	737	741
Y	21.1	23.1	19.3	20.0	22.7	21.5	19.6	20.5
Zr	166	183	136	163	194	324	171	201
Nb	28.0	31.2	20.8	22.8	31.3	52.5	26.4	27.9
Cs	0.2	0.2	0.2	0.1	0.3	0.2	0.2	0.1
Ba	234	185	127	125	252	205	191	168
La	22.1	24.7	18.2	17.8	23.0	44.7	21.6	22.8
Ce	46.4	51.8	37.5	37.7	48.9	91.9	45.6	50.3
Pr	6.02	6.76	5.17	5.15	6.72	12.10	6.05	6.65
Nd	25.3	30.1	22.1	22.8	28.7	47.7	26.1	28.2
Sm	5.30	6.16	4.97	5.06	6.16	9.55	5.44	5.90
Eu	1.85	2.18	1.84	1.93	2.16	3.18	1.95	2.05
Gd	5.05	5.72	4.78	4.96	5.83	7.99	5.00	5.31
Tb	0.81	0.90	0.75	0.79	0.90	1.11	0.80	0.83
Dy	4.21	4.90	4.20	4.07	4.57	5.28	3.95	4.24
Ho	0.72	0.83	0.67	0.73	0.75	0.77	0.68	0.75
Er	1.96	2.05	1.76	1.77	1.94	1.81	1.68	1.88
Tm	0.27	0.29	0.24	0.24	0.28	0.22	0.23	0.27
Yb	1.59	1.60	1.30	1.37	1.48	1.14	1.26	1.26
Lu	0.22	0.23	0.19	0.20	0.23	0.17	0.19	0.21
Hf	4.5	4.8	4.0	3.9	4.6	7.9	4.1	5.0
Ta	1.7	1.7	1.2	1.3	2.0	3.1	1.6	1.8
Pb	0.6	1.5	0.9	1.0	1.5	2.4	1.5	1.0
Th	2.8	2.6	1.9	1.8	1.8	4.7	3.9	1.7
U	0.8	0.7	0.6	0.6	0.6	1.4	0.7	0.8

17

18

19

Sample	DO-59 (O-1)	DO-60 (O-1)	DO-61 (O-1)	DO-62 (O-2)	DO-63 (O-1)	DO-64 (O-3)	DO-65 (O-3)
Latitude	37°41'24.84"N	37°41'24.72"N	37°42'28.50"N	37°41'5.04"N	37°41'42.24"N	37°39'11.34"N	37°39'8.35"N
Longitude	40° 1'10.20"E	40° 1'13.14"E	40° 3'25.68"E	40° 3'46.80"E	40° 4'7.08"E	40° 0'4.38"E	40° 0'13.52"E
SiO ₂	47.29	47.21	44.82	46.50	47.41	44.18	43.64
TiO ₂	2.31	2.42	2.84	2.67	2.47	3.32	3.22
Al ₂ O ₃	13.22	13.38	13.54	14.53	13.61	13.43	13.10
Fe ₂ O ₃	12.78	13.17	14.23	13.66	13.17	14.91	14.42
MgO	10.44	10.37	9.11	8.22	9.88	9.95	9.75
MnO	0.16	0.16	0.17	0.17	0.16	0.18	0.17
CaO	8.55	8.25	9.00	8.98	8.35	9.10	8.83
Na ₂ O	3.06	3.09	3.44	3.45	3.06	4.03	4.08
K ₂ O	1.21	1.26	1.51	1.51	1.27	1.80	1.69
P ₂ O ₅	0.43	0.44	0.67	0.47	0.46	0.70	0.71
Cr ₂ O ₃	0.049	0.047	0.035	0.038	0.044	0.032	0.032
LOI	0.1	-0.2	0.2	-0.2	-0.3	0.0	-0.1
Total	99.64	99.64	99.60	99.65	99.63	101.65	99.56
Ni	242	245	178	110	231	181	174
Sc	21	21	21	21	21	19	19
V	229	233	253	260	237	267	255
Co	70.4	72.1	70.4	64.6	72.9	82.5	72.2
Cu	41.9	54.9	60.1	46.3	54.5	52.1	49.2
Zn	65	86	106	91	85	94	69
Ga	20.6	21.4	22.7	22.4	22.1	24.9	25.0
Rb	18.1	17.4	14.5	14.0	17.7	15.7	15.3
Sr	568	602	894	678	610	949	934
Y	20.0	21.5	24.0	24.4	21.8	24.7	24.4
Zr	162	173	219	187	178	267	255
Nb	26.3	27.9	41.1	30.9	29.4	57.2	55.5
Cs	0.8	0.7	0.2	0.3	0.8	0.2	0.2
Ba	202	221	234	216	228	258	261
La	23.1	25.4	37.8	27.3	25.9	41.8	41.3
Ce	48.3	52.3	76.5	56.5	53.0	86.0	83.9
Pr	6.14	6.55	9.61	7.32	6.84	10.87	10.71
Nd	25.2	27.8	40.0	31.6	28.2	44.7	44.4
Sm	5.33	5.65	7.64	6.13	5.78	8.56	8.31
Eu	1.90	1.93	2.59	2.27	1.98	2.86	2.74
Gd	5.35	5.74	7.44	6.31	5.83	8.13	7.82
Tb	0.82	0.86	1.09	0.94	0.88	1.14	1.01
Dy	4.18	4.42	5.10	4.91	4.60	5.42	5.27
Ho	0.76	0.81	0.90	0.90	0.83	0.93	0.89
Er	1.83	1.91	2.16	2.18	1.98	2.10	2.05
Tm	0.27	0.30	0.29	0.33	0.31	0.31	0.30
Yb	1.55	1.59	1.67	1.87	1.66	1.70	1.64
Lu	0.25	0.28	0.28	0.30	0.28	0.27	0.26
Hf	4.1	4.3	5.6	4.8	4.5	6.7	6.3
Ta	1.6	1.7	2.5	1.9	1.8	3.4	3.2
Pb	2.1	3.3	2.7	2.7	2.8	2.6	2.3
Th	3.0	3.2	3.4	3.0	2.9	3.6	3.6
U	1.1	0.9	1.0	0.9	0.8	1.3	1.3

20

21

22

Sample	DO-66 (O-3)	DO-67 (O-3)	DO-68 (O-1)	DO-69 (O-1)	DO-70 (O-1)	DO-71 (O-1)	DO-72 (O-1)
Latitude	37°39'7.20"N	37°39'7.62"N	37°42'28.62"N	37°40'13.44"N	37°39'10.86"N	37°38'13.32"N	37°36'56.58"N
Longitude	40° 0'29.10"E	40° 0'29.34"E	40° 8'10.98"E	39°59'10.38"E	39°58'49.08"E	39°58'14.22"E	39°58'44.58"E
SiO ₂	44.48	44.95	46.28	47.06	46.92	47.26	47.18
TiO ₂	2.88	2.73	2.76	2.78	2.68	2.52	2.44
Al ₂ O ₃	13.14	13.22	13.97	14.24	13.26	13.23	13.37
Fe ₂ O ₃	14.76	14.29	13.55	13.89	14.28	13.36	13.65
MgO	9.52	9.66	9.44	9.73	9.57	10.06	10.01
MnO	0.17	0.17	0.16	0.17	0.16	0.16	0.16
CaO	8.57	8.61	8.25	8.35	8.09	8.34	8.24
Na ₂ O	3.94	3.77	3.37	3.46	3.34	3.27	3.17
K ₂ O	1.74	1.62	1.33	1.38	1.36	1.20	1.19
P ₂ O ₅	0.71	0.61	0.53	0.56	0.48	0.43	0.44
Cr ₂ O ₃	0.032	0.035	0.046	0.047	0.035	0.045	0.043
LOI	-0.4	-0.1	-0.1	0.0	-0.6	-0.3	-0.3
Total	99.57	99.60	99.62	101.69	99.61	99.62	99.62
Ni	176	191	194	213	227	235	234
Sc	19	20	19	20	19	20	20
V	240	235	242	247	229	233	218
Co	74.5	74.3	69.8	73.5	77.5	73.1	75.5
Cu	45.1	49.1	53.9	52.1	65.5	58.9	57.6
Zn	99	65	88	92	95	92	89
Ga	24.5	22.8	21.2	22.3	23.7	21.4	21.7
Rb	19.1	18.7	13.8	14.7	16.1	16.6	15.4
Sr	878	814	705	762	663	625	613
Y	24.7	24.4	20.5	21.6	22.0	22.1	22.4
Zr	240	235	242	203	197	172	175
Nb	52.8	47.0	27.5	27.9	29.7	29.1	29.5
Cs	0.4	0.4	0.2	0.2	0.5	0.5	0.5
Ba	272	254	209	224	187	209	201
La	43.2	37.0	28.6	29.8	28.6	26.3	26.7
Ce	85.1	72.9	58.4	59.9	56.4	52.0	52.1
Pr	10.67	9.39	7.4	7.65	7.37	6.90	6.69
Nd	42.7	37.4	31.8	32.1	31.1	28.6	28.6
Sm	8.01	7.08	5.92	6.11	6.26	5.75	5.68
Eu	2.73	2.41	2.15	2.18	2.15	2.02	2.03
Gd	7.81	7.09	5.88	5.91	6.18	5.73	5.90
Tb	1.11	1.03	0.85	0.85	0.93	0.88	0.89
Dy	5.41	5.07	4.20	4.50	4.57	4.50	4.60
Ho	0.94	0.90	0.75	0.80	0.84	0.79	0.83
Er	2.15	2.15	1.83	1.92	1.98	1.93	1.91
Tm	0.32	0.32	0.28	0.28	0.28	0.29	0.30
Yb	1.81	1.75	1.48	1.57	1.51	1.64	1.67
Lu	0.29	0.28	0.24	0.30	0.25	0.26	0.26
Hf	6.2	5.7	5.1	4.9	5.3	4.6	4.4
Ta	3.1	2.7	1.7	1.8	1.9	1.8	1.8
Pb	2.1	2.1	1.0	1.0	3.0	2.4	2.6
Th	4.5	3.7	2.3	2.7	3.3	2.9	3.0
U	1.4	1.2	0.8	0.9	1.1	0.9	0.9

23

24

25

26

Sample	DO-73 (O-1)	DO-74 (O-1)	DO-75 (O-1)	DO-76 (O-1)	DO-77 (O-3)	DO-78 (O-3)	DO-107 (O-1)
Latitude	37°36'33.96"N	37°35'56.46"N	37°35'45.84"N	37°35'51.18"N	37°37'10.86"N	37°37'47.04"N	37°37'1.62"N
Longitude	39°59'11.46"E	39°59'40.14"E	40° 1'12.00"E	40° 3'33.96"E	40° 4'45.36"E	40°10'58.26"E	39°58'37.74"E
SiO ₂	47.05	47.80	45.68	47.31	44.05	45.88	46.73
TiO ₂	2.35	2.40	2.62	2.53	3.31	2.43	2.50
Al ₂ O ₃	13.39	13.50	13.35	13.25	12.58	12.79	13.62
Fe ₂ O ₃	14.12	13.36	13.63	13.25	14.74	13.63	13.22
MgO	10.27	10.17	10.29	10.01	10.59	11.25	10.35
MnO	0.16	0.16	0.17	0.16	0.18	0.17	0.17
CaO	8.71	8.07	8.69	8.36	9.47	8.73	8.56
Na ₂ O	3.16	3.27	3.34	3.36	3.55	3.16	3.12
K ₂ O	1.08	1.13	1.30	1.22	1.45	1.20	1.23
P ₂ O ₅	0.40	0.39	0.53	0.47	0.70	0.46	0.44
Cr ₂ O ₃	0.041	0.045	0.042	0.044	0.038	0.043	0.046
LOI	-0.6	-0.7	-0.1	-0.4	0.0	-0.2	-0.4
Total	99.64	99.64	99.58	99.61	100.69	99.58	99.64
Ni	241	255	213	234	227	251	246
Sc	21	21	21	20	21	21	21
V	215	213	225	215	267	221	221
Co	73.9	68.8	76.9	70.1	74.2	71.3	78.4
Cu	61.5	59.2	46.0	60.0	56.3	57.7	50.2
Zn	89	87	101	87	105	91	80
Ga	20.8	21.9	21.0	22.1	23.3	20.7	21.0
Rb	13.4	14.5	15.4	16.2	12.8	15.3	15.3
Sr	546	503	752	582	886	637	583
Y	20.9	20.3	21.7	21.8	23.9	20.8	20.0
Zr	158	158	184	183	228	168	173
Nb	24.1	23.4	36.8	31.6	50.8	34.7	29.4
Cs	0.2	0.3	0.3	0.5	0.2	0.2	0.5
Ba	164	167	235	197	291	377	212
La	22.5	18.7	26.8	22.3	35.8	22.8	22.4
Ce	45.3	41.5	59.3	51.0	77.2	51.0	47.1
Pr	6.02	5.37	7.44	6.43	9.67	6.50	6.44
Nd	25.2	22.1	30.5	27.7	38.6	27.2	27.7
Sm	5.33	5.06	6.27	5.92	7.90	5.50	5.96
Eu	1.86	1.82	2.09	1.95	2.67	1.94	1.90
Gd	5.35	5.38	6.09	5.98	7.65	5.51	5.56
Tb	0.86	0.85	0.90	0.89	1.07	0.83	0.84
Dy	4.56	4.23	4.60	4.44	5.13	4.30	4.21
Ho	0.80	0.75	0.80	0.82	0.87	0.77	0.78
Er	1.88	1.78	2.04	1.94	2.09	1.89	1.99
Tm	0.28	0.26	0.27	0.27	0.29	0.28	0.24
Yb	1.58	1.49	1.53	1.49	0.22	1.52	1.49
Lu	0.26	0.22	0.23	0.22	0.22	0.24	0.21
Hf	4.2	4.1	4.6	4.7	5.7	4.3	4.7
Ta	1.4	1.4	2.2	2.0	3.0	2.0	1.9
Pb	2.4	2.5	2.5	3.8	2.0	2.3	2.1
Th	2.5	2.2	3.4	3.4	3.6	3.3	2.7
U	0.7	0.4	1.0	0.9	1.1	0.8	0.7

27

Sample	DO-108 (O-1)	DO-109 (O-1)	DO-110 (O-2)	DO-113 (O-2)	DO-114 (O-3)	DO-117 (O-3)	DO-120 (O1)
Latitude	37°38'19.56"N	37°43'0.90"N	37°43'27.18"N	37°41'6.34"N	37°40'17.88"N	37°37'32.52"N	37°38'4.98"N
Longitude	39°58'16.20"E	40° 0'6.54"E	40°15'38.34"E	40°10'23.70"E	40°13'52.50"E	40° 9'36.66"E	40° 6'7.80"E
SiO ₂	47.03	45.14	47.60	48.37	45.07	42.12	47.50
TiO ₂	2.47	2.80	2.04	2.26	2.76	3.27	2.25
Al ₂ O ₃	13.39	13.50	14.35	13.87	13.12	12.20	13.41
Fe ₂ O ₃	13.38	13.52	13.74	13.45	13.65	14.96	13.64
MgO	10.10	9.13	9.12	8.81	10.42	10.50	9.72
MnO	0.17	0.17	0.17	0.17	0.18	0.19	0.17
CaO	8.32	9.06	8.52	8.33	9.15	9.91	8.25
Na ₂ O	3.20	3.53	2.88	3.26	3.15	3.44	3.24
K ₂ O	1.23	1.48	0.72	1.12	1.50	1.60	1.29
P ₂ O ₅	0.45	0.59	0.28	0.36	0.62	0.81	0.41
Cr ₂ O ₃	0.046	0.038	0.046	0.044	0.038	0.039	0.040
LOI	-0.2	0.7	0.2	-0.4	-0.1	0.5	-0.3
Total	99.63	99.65	99.67	99.67	99.59	99.53	99.64
Ni	241	185	185	165	221	220	207
Sc	21	21	23	23	22	21	21
V	238	247	229	227	260	279	213
Co	77.2	70.9	76.8	66.7	88.9	86.9	68.7
Cu	49.9	48.0	37.3	40.2	44.3	51.0	43.0
Zn	81	94	77	79	75	90	88
Ga	22.0	23.8	21.1	20.9	22.3	23.0	19.2
Rb	16.5	15.6	5.6	17.3	19.1	17.4	17.5
Sr	604	766	401	487	859	961	537
Y	20.9	22.2	20.7	20.9	23.2	23.7	21.3
Zr	180	202	137	156	211	235	164
Nb	30.6	36.4	16.0	21.7	48.1	56.0	29.0
Cs	0.5	0.2	0.1	0.2	0.2	0.2	0.4
Ba	217	207	225	205	294	301	220
La	23.2	29.5	15.9	20.3	34.6	38.7	22.5
Ce	48.5	62.1	34.8	43.6	70.0	79.7	46.7
Pr	6.56	8.24	4.74	5.87	9.00	10.38	6.07
Nd	28.8	34.5	21.8	26.0	37.0	45.0	27.1
Sm	6.02	7.10	4.85	5.50	7.44	8.29	5.57
Eu	1.87	2.25	1.55	1.68	2.23	2.64	1.74
Gd	5.58	6.35	4.66	5.04	6.56	7.31	5.30
Tb	0.89	0.99	0.77	0.83	0.95	1.08	0.83
Dy	4.24	4.85	4.04	4.29	4.69	5.03	4.51
Ho	0.81	0.84	0.78	0.84	0.84	0.85	0.85
Er	2.13	2.11	2.19	2.13	2.29	2.03	2.02
Tm	0.27	0.29	0.29	0.29	0.30	0.28	0.28
Yb	1.47	1.58	1.63	1.72	1.54	1.51	1.70
Lu	0.21	0.21	0.26	0.26	0.24	0.23	0.25
Hf	4.3	5.6	4.0	4.7	5.3	6.1	4.4
Ta	2.0	2.2	1.1	1.4	2.9	3.3	1.8
Pb	1.6	1.2	1.9	1.5	2.2	2.2	2.2
Th	2.4	2.4	3.0	4.2	4.4	5.5	2.9
U	0.9	1.0	0.3	0.6	1.2	1.4	0.8

Table 2: Karacadağ and Ovabağ Isotopic Results

Sample	$^{143}\text{Nd}/^{144}\text{Nd}$	$^{87}\text{Sr}/^{86}\text{Sr}$	$^{206}\text{Pb}/^{204}\text{Pb}$	$^{207}\text{Pb}/^{204}\text{Pb}$	$^{208}\text{Pb}/^{204}\text{Pb}$
DK-1 (K-1)	0.512863	0.703687	19.032	15.616	38.823
DK-10 (K-1)	0.512916	0.703321			
DK-19 (K-1)	0.512880	0.703303			
DK-23 (K-2)	0.512856	0.703484	19.018	15.615	38.816
DK-25 (K-3)	0.512924	0.703065	19.113	15.552	38.728
DK-27 (K-3)	0.512933	0.703095			
DK-29 (K-2)	0.512881	0.703379	19.130	15.595	38.874
DK-52 (K-2)	0.512878	0.703683			
DK-58 (K-1a)	0.512657	0.704303	18.873	15.636	38.828
DO-59 (O-1)	0.512794	0.704063	18.948	15.628	38.752
DO-62 (O-2)	0.512816	0.703722	18.832	15.606	38.729
DO-64 (O-3)	0.512928	0.703235			
DO-67 (O-3)	0.512880	0.703501			
DO-68 (O-1)	0.512864	0.703726	18.989	15.594	38.820